THESIS

EVALUATION OF A NON-THERMAL PLASMA GENERATOR FOR PLASMA-ASSISTED

COMBUSTION IN AN OIL BURNER

Submitted by

Jake Downin Doyle

Department of Mechanical Engineering

In partial fulfillment of the requirements

For the Degree of Master of Science

Colorado State University

Fort Collins, Colorado

Spring 2013

Master's Committee:

      Advisor: Azer Yalin
      Co-Advisor: Sachin Joshi

      Anthony Marchese
      George Collins

ABSTRACT

EVALUATION OF A NON-THERMAL PLASMA GENERATOR FOR PLASMA-ASSISTED

COMBUSTION IN AN OIL BURNER

The addition of plasma to a combustion system has the potential to increase the combustion efficiency and reduce harmful emissions by reforming hydrocarbon fuels. The ability for plasma to reform fuel to create hydrogen-rich synthesis gas has been shown by other researchers. The work presented in this thesis includes the characterization of a plasma generator patented by Clean Diesel, LLC and testing an oil burner that was modified to use the plasma generator for combustion enhancement. The plasma was generated by six electrodes with a circulating high voltage pulse created by a signal generator and high voltage transformers. The plasma is characterized through optical emission spectroscopy and with electrical measurements, where it was shown to be a non-thermal plasma operating in the glow-to-arc transition region. The plasma generator was then implemented into an oil burner where its thermal efficiency and emissions were compared to that of a stock Riello F10 burner. Testing showed similar efficiencies for the modified and stock burners (contrary to previous testing that showed improvements due to plasma assistance). Carbon monoxide and nitrogen oxides were considered as the key pollutants, and it was shown that NOx emissions exceeded that of the stock burner, although CO levels were reduced. Further testing was performed with additional modifications such as fuel spray type, electrode insulation, and plasma frequency, although none showed significant improvements in its operation. The results have led to the realization that a more

volumetric plasma that can provide longer residence time for fuel interaction is likely needed for

effective fuel reforming.

ACKNOWLEDGEMENTS

TABLE OF CONTENTS

LIST OF TABLES

LIST OF FIGURES

xi

Chapter 1

Introduction

Plasma fuel reforming is an emerging technology that has the potential to improve the performance of combustion systems. The goal of the technology is to capitalize on plasma chemistry that enhances the combustion process. Plasma is a fourth state of matter where molecules and atoms are partially ionized, which produces free electrons and other new species. The free electrons move very fast and have much more kinetic energy compared to the other atoms and molecules, thereby causing disassociation of other molecules by electron impact [1]. This creates a rather interesting possibility when considered for the breakdown of fuel molecules. After all, the combustion process itself consists of chemical reactions that break fuel structures down into smaller molecules and radicals. Plasma fuel reforming is the process of using plasma to ionize fuel molecules to create products that combust more effectively [2], thereby increasing combustion efficiency and possibly reducing harmful emissions such as carbon-monoxide (CO), nitrogen-oxides (NO, NO_2), and particulate matter (PM).

Plasma fuel reforming is being considered for many applications such as engines, most notably internal combustion engines for automobiles. This project deals with one of the simplest combustion machines: the oil burner. There is room for improvement in the oil burner industry, and the oil burner also serves as a relatively simple testing device due to atmospheric pressure conditions, ease of installment and modification, and inexpensiveness. The oil burner is a device that combines fuel, air, and an ignition source to cause combustion to elevate water temperatures

in a boiler or furnace. The furnace used in this research will be referred to as a boiler (though it does not heat water to its boiling temperature). The current research addresses the fuel reforming capabilities of a plasma generator provided by Clean Diesel LLC, a start-up company originally formed in Massachusetts. The plasma generator is first characterized via electrical and spectroscopic measurements, and then tested in a modified oil burner to determine the benefits of a plasma-assisted burner with respect to a typical spark-ignited burner.

The introductory chapter provides details on the concepts that are used for plasma characterization and plasma fuel reforming. In Section 1.1, plasmas will be explained in further detail as far as different types and their thermal properties. The defining parameters and measurement techniques will be explained, as well as a review of previous work in plasma diagnostics. Then, the process of plasma fuel reforming is explained in detail, including chemical kinetics and the production of syngas in Section 1.2. A literature review of other work in plasma fuel reforming is also included. Finally, the research objectives are reviewed to sum up the motivations and goals of the research in Section 1.3.

1.1 Overview of Processing Plasmas

Plasma is a macroscopically neutral state of matter consisting of free electrons along with ionized atoms and/or molecules [3]. Upon the addition of large amounts of energy, such as heat, electrons are able to overcome the atomic or molecular binding energy via collisions to free themselves. Ionization occurs because of the high energy density of the plasma; electrons become energetic enough to separate from atoms, creating positively and negatively charged molecules and atoms (ions). This collection of charged particles also makes plasma a strong

electrical conductor, which can be influenced by electromagnetic forces. As a whole, plasma is collectively neutral despite its varying internally charged particles and it exhibits collective behavior. Plasma is a very complex state of matter due to the electric and magnetic interactions between free electrons, ions, neutral particles, and photons. Plasma is characterized primarily by its density and temperature. Temperature is a way of describing the energy of the electrons, ions, atoms, and molecules within the plasma. In a non-thermal plasma, there are several temperatures including electron, ion, vibrational, and rotational temperatures, which are not necessarily the same. There are multiple types of plasmas that are defined by differences in these mentioned properties.

The plasmas of interest here are man-made plasmas, typically created by application of electrical power. A simple way of creating plasma is to apply a voltage difference between an anode and cathode. When the anode and cathode are separated by a suitable distance, plasma can be formed when the electric field becomes strong enough. The medium between the electrodes, such as air, becomes ionized at this point and allows electrons to flow from the cathode to the anode. Photons are typically emitted from the plasma, allowing it to be seen by the human eye.

1.1.1 Thermal and Non-Thermal Plasmas

Plasmas can be categorized as either thermal or non-thermal. A thermal plasma, also known as an equilibrium plasma, consists of ions, electrons, and neutral species having a single temperature (kinetic energy). A non-thermal, or non-equilibrium, plasma contains electrons that are at a much higher temperature than the ions and other species [4]. Although the electron temperature is very high, the majority of the plasma mass is made up of the cooler ions. This

3

means that a non-thermal plasma can exist at temperatures as low as room temperature. On the other hand, thermal plasmas typically have an equilibrium temperature between the electrons and ions which can be several thousand degrees Kelvin or higher [2].

1.1.2 Plasma Regimes

<u>Corona Discharge</u>

The corona discharge is an example of a non-thermal plasma which can be formed at or near atmospheric pressure. A corona is formed with a visible ionization region from an asymmetrical pair of electrodes (such as a point-to-plane configuration) [5,6]. This plasma requires the least amount of voltage and current between electrodes. Ionization occurs in the region near the charged electrode, but its low strength prevents the formation of an arc to the anode. The more distant regions from the electrode neutralize the ionization field. The corona discharge can be visually described as having many streams of visible light that are not necessarily uniform in their composition. An example of a corona discharge is shown in Figure 1-1 [7].

Figure 1-1: Example of a corona discharge [7].

<u>Glow Discharge</u>

The glow discharge is another non-thermal plasma, and is the plasma regime formed after corona with increasing current. As voltage is increased across a cathode-anode pair, the plasma reaches a breakdown voltage which suddenly sees a drop in voltage and increase in current, meaning that the region between electrodes is more ionized and current is flowing through the medium between electrodes [8]. The glow discharge is distinguished by its high-voltage, low-current (compared to the arc discharge) formation. The general composition of a glow plasma is shown in Figure 1-2 [9].
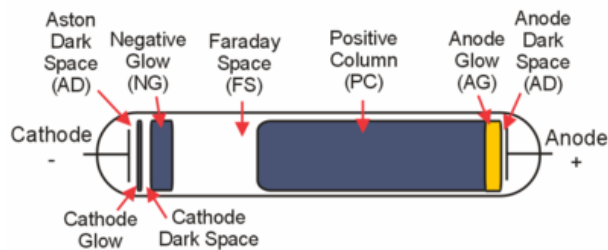
Figure 1-2: Composition of a typical glow plasma [9].

Arc Discharge

The arc discharge is distinguished by its formation under low-voltage, high current conditions. The arc is formed by increasing the current of the glow discharge. As voltage is increased in the glow regime, another breakdown voltage point is reached, which once again shows a sudden drop in voltage with an increase in current. At this point, the medium between electrodes is close to full ionization. The arc discharge is seen often, such as in a lightning bolt or welding arc, and is typically considered a thermal plasma. An example of an arc discharge is shown in Figure 1-3 [10].
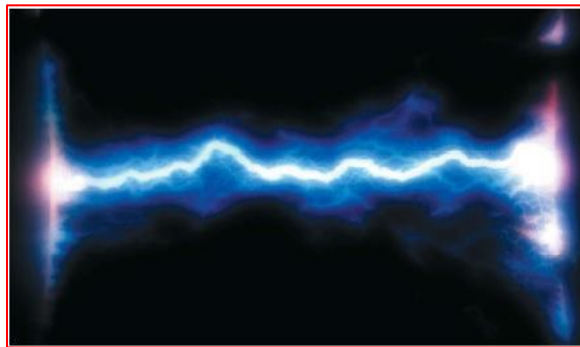
Figure 1-3: Example of an arc discharge [10].

The relationship between voltage and current for the different plasma regimes are shown in Figure 1-4 [11].
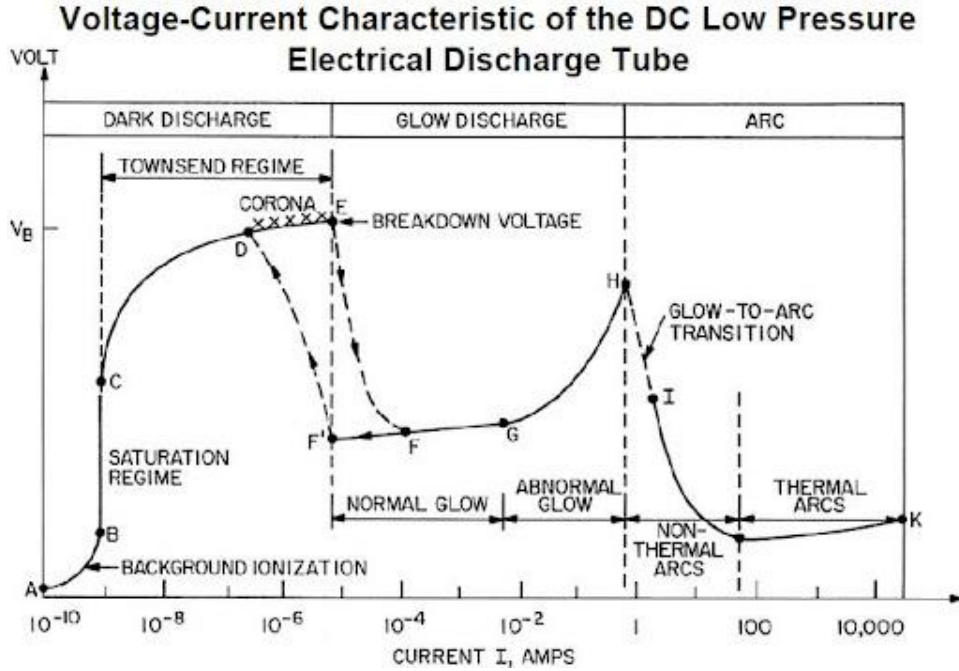
Figure 1-4: Diagram of plasma regimes for DC excitation within discharge tube [11].

1.1.3   Main Plasma Parameters

The plasma parameters that are most important to the characterization of a plasma are the electron density (n_e), the electron temperature (T_e), and ion temperature (T_i). The electron density refers to the number of electrons per unit volume [12], and the electron and ion temperatures were mentioned previously. Vibrational and rotational temperatures $(T_{vib}$ and $T_{rot})$ describe the energy of molecules within the plasma, and they can be explained with a brief review of quantum physics. In a diatomic molecule, such as N_2, there are electronic energy levels that represent the energy of electrons. The discrete energy levels permit only certain transitions that absorb or emit a photon of a specified wavelength, i.e., energy. For a transition from an arbitrary level q to level p, the energy can be expressed as $E = E_q - E_p$. Within the molecule, there

7

are vibrational levels within an electronic level that corresponds to the energy of the vibrations of the molecular bond. Just as in the electronic state, there are discrete energy levels (bands) that represent vibrational energies. The next step is the consideration of rotational energy corresponding to the rotation of two (for diatomic) atoms within the molecule. The rotational energies are similarly in discrete energy levels within the vibrational levels. Transitions can occur between energy levels located in the electronic, vibrational, and rotational states; each transition corresponding to a specific wavelength of an emitted photon. An energy level diagram of the N_2 molecule is shown in Figure 1-5 [13].
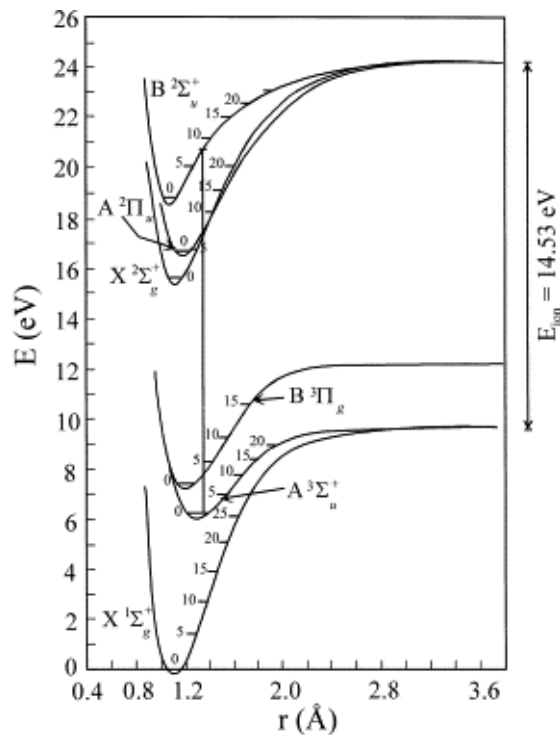
Figure 1-5: Energy level diagram of the N_2 molecule [13].

These energies can then be expressed in terms of temperature. For non-thermal plasmas, it can be assumed that the rotational temperature is approximately equal to the gas temperature,

T_g, [14] due to its correlation to the molecule itself, rather than the electrons. For non-thermal plasmas, it is typical for the temperatures to be related as follows [4]:

$$T_e > T_{vib} > T_{rot} = T_g \qquad (1.1)$$

It can be shown that a plasma is non-thermal if the temperatures follow this rule.

1.1.4 Measurement Techniques of Plasma Parameters

A common method for measuring some of the noted plasma parameters is through the use of a Langmuir probe. It allows the electron density, electron temperature, and electric field to be measured [15], but it is an intrusive method of measurement requiring the probe to be inserted into the plasma. The plasma parameters in this project were measured by spectroscopic techniques.

Optical Emission Spectroscopy (OES) is an established technique to characterize plasma parameters via the collection of emission spectra [16]. Transitions between energy levels emit photons that can be dispersed by a spectrometer to provide specific wavelengths and corresponding intensities. The collected spectrum is dependent on the molecular or atomic species that are involved and the plasma conditions. Since only the emitted light is required for this analysis, it is a non-intrusive measurement procedure that allows for the characterization of the plasma under its operating conditions.

OES records light emitted from the atoms and molecules that compose the plasma where specific wavelengths represent atomic and molecular transitions. A comprehensive list of

transitions and corresponding wavelengths can be found in the NIST database [17], which is a very useful tool in analyzing emission spectra. The presence of certain wavelengths shows what species are present in the plasma, and the intensities and broadening effects of specific transitions can provide information regarding plasma temperatures and densities.

The process of finding vibrational and rotational temperatures has been described well by Staack et al. [4,18] and Laux et al. [14]. The process of determining these temperatures primarily is based upon the second positive system of nitrogen. Vibrational and rotational temperatures can be determined by comparing experimentally collected spectra to that of modeled spectra. SPECAIR is a computer model that simulates emission spectra in the ultraviolet (UV) to near infrared (NIR) range [4]. By providing the program with inputs such as the composition of the medium (such as air), and predetermined values for electronic, vibrational, rotational, and translational temperatures, a modeled spectrum is plotted. In this way, experimental spectra can be compared to modeled spectra to determine plasma temperatures. Relative intensities of vibrational transitions lead to values of T_{vib}, while the relative intensities of rotational lines (which generally make up the tails of vibrational lines) lead to T_{rot}. Most of the transitions that aid in this analysis are located between 292 and 376 nm, which are described in more detail in Chapter 3.

The electron density and electron temperature can be found through the Stark broadening of hydrogen lines. Stark broadening is a result of the Stark effect, which broadens spectral lines because of the interaction of atoms with free electrons and ions in the electric field created by the plasma. This broadening is heavily influenced by T_e and n_e. Torres et al. [19,20] used a method to simultaneously determine both of these parameters by looking at the Balmer series lines, H_α, H_β, and H_γ. With Stark broadening measurements of at least two of these lines, a crossing-point

method can be performed to find T_e and n_e. To see the Balmer series lines, it is typically a requirement to add at least 1% hydrogen to the plasma which has very little effects outside of allowing these lines to be seen [19]. The Stark broadening of a spectral line is combined with other broadening mechanisms that must be deconvoluted in order to determine the Stark broadening on its own. These other mechanisms include Doppler, van der Waals, instrumental, natural, and resonant broadening. The latter two mechanisms can generally be neglected due to their small effect [19], but the others must be calculated, or in the case of instrumental broadening, be measured experimentally. Instrumental broadening is a result of the spectrometer and its components increasing the width of a spectral line. Doppler and van der Waals broadening can be calculated with equations based on the spectral line being examined, mass of the emitting atom or molecule, the gas temperature, and the neutral density of the plasma [21]. The convolution of all mechanisms results in a Voigt profile of the experimental lineshape. The Stark broadening value can be separated from this width as a Lorentzian profile. By examining the T_e and n_e relationships of each Balmer series line, the intersection of the three curves represent the actual T_e and n_e of the plasma.

Another method of finding the electron density using only the H_β line was performed by Laux et al. [14]. This method is possible for plasmas with electron densities greater than 5 x 10^{-13} cm^{-3} and uses a similar analysis of the Stark broadening of the H_β line, but one can solve for n_e using only this line because the broadening has a weak correlation with electron temperature. A final approach to find T_e and n_e, albeit a less accurate one, is to find the Stark broadening from only the H_α line [21,22] using tabulated relationships between T_e, n_e, and Stark broadening widths.

1.2 Plasma Fuel Reforming

Plasma fuel reforming and plasma assisted combustion are topics of great recent interest, due to the need for more efficient use of fossil fuels and stricter emissions regulations. It is well known that hydrogen is one of the best combustion fuels due to its high heating value (120 kJ/g), but its storage characteristics make it very difficult to use, especially for mobile vehicles [2]. These characteristics include its low density and high flammability, meaning that vehicles would require massive storage tanks of hydrogen to travel moderate distances which could result in disaster in the case of automobile accidents. One method to use hydrogen as a fuel is to produce it on site via commonly used liquid fuels such as gasoline or diesel. This process is known as fuel reforming, and can be achieved with the use of plasma. Another aspect of the reforming process is to use plasma as a method of adding energy into fuel to initiate formation of radicals early in the combustion process [23-27]. Chain reactions are essential to combustion processes by producing highly reactive radical species that create chain-propagating reactions that turn the reactants (fuel and oxidizer) into final products like water and carbon dioxide [28]. Plasma can be used to artificially start chain-initiation reactions to shorten ignition delay and cause more complete combustion. Advancements in plasma fuel reforming technology can potentially decrease large-scale fuel consumption and reduce harmful emissions while continuing use of the existing fuel distribution network.

1.2.1 Syngas Production

Synthesis gas, or syngas, is a mixture of hydrogen (H_2) and carbon monoxide (CO). The intention of most fuel reforming technologies is to produce syngas from hydrocarbon fuels. Syngas can be produced from chemical reactions involving a hydrocarbon and an oxidizer. The oxidizer can be oxygen, water, and even carbon dioxide. Petitpas et al. [2] shows that the oxidation can occur in the following reactions:

$$\text{Partial Oxidation:} \quad C_nH_m + \frac{n}{2}O_2 \rightarrow nCO + \frac{m}{2}H_2 \qquad (1.2)$$

$$\text{Steam Reforming:} \quad C_nH_m + nH_2O \rightarrow nCO + \left(\frac{m}{2} + n\right)H_2 \qquad (1.3)$$

$$\text{Dry } CO_2 \text{ Reforming:} \quad C_nH_m + nCO_2 \rightarrow 2nCO + \frac{m}{2}H_2 \qquad (1.4)$$
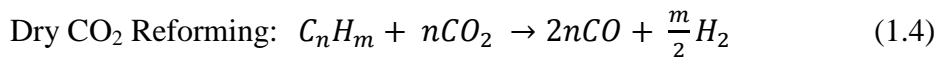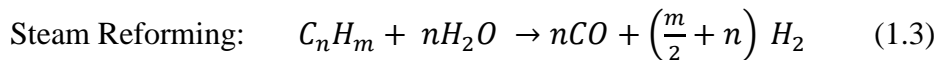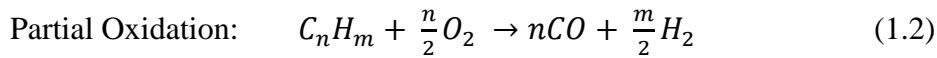
A water gas shift reaction can then convert the CO into CO_2 and additional hydrogen:

$$\text{Water Gas Shift Reaction:} \quad H_2O + CO \rightarrow H_2 + CO_2 \qquad (1.5)$$
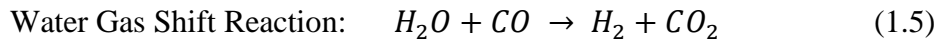
Catalysts have previously been used to allow these reactions to take place, but it has been shown that plasma can be used to improve this process to eliminate problems associated with catalysts such as soot poisoning, low efficiency, and cost [2]. Plasma benefits the reforming process by introducing highly reactive species such as free electrons and ions that enhance these chemical reactions. The downside of plasma assistance is that it requires energy to create it. If the gains in efficiency due to the plasma reformer are equal to or less than the additional power required for its operation, than the concept is not useful. In this regard, use of non-thermal

plasmas with low power consumption can be attractive. With the high electron temperatures and low gas temperatures of non-thermal plasmas, power consumption can remain low while having a significant impact on the reforming process by creating radicals and excited species [29]. Because non-thermal plasmas are complex, the chemistry related to its reaction with fuel is very hard to predict, and most research has made conclusions based on experimental results rather than theoretical calculations [2].

1.2.2 Plasmatron

The Massachusetts Institute of Technology's Plasma Science and Fusion Center has performed a great deal of research related to plasma fuel reforming technology [30-33]. MIT researchers have developed the Plasmatron, a device designed to produce hydrogen-rich fuel from mixtures of air/water and hydrocarbons. A schematic of a version of the Plasmatron is shown in Figure 1-6.
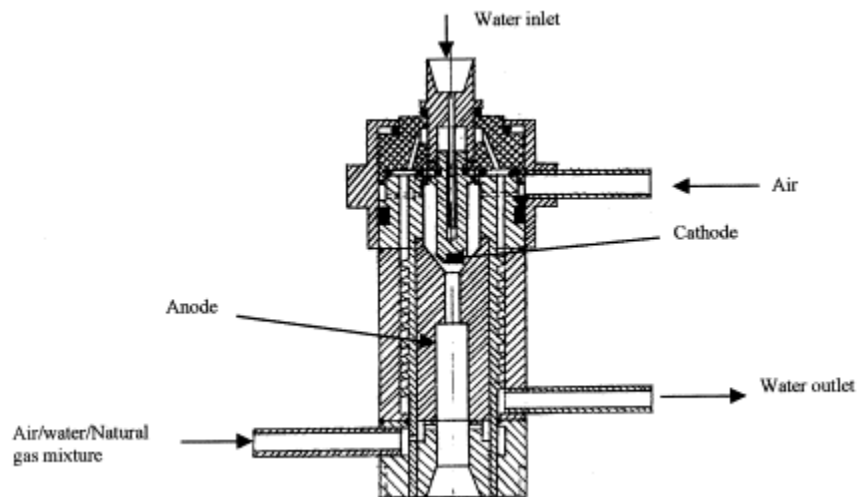
Figure 1-6: Schematic of MIT's Plasmatron [30].

14

Diesel was used as the fuel in a particular experiment [30], which was injected with air and water into the Plasmatron. After the fuel/oxidizer mixture interacts with the plasma, it flows to a catalyst which further enhances the chemical reactions. Gas samples were recorded to determine the composition of the reformate. Tests were performed regarding the preheating of the diesel, air, and/or water before injection into the Plasmatron. Results of the testing showed no evidence of soot and the production of up to 30% H_2 and 20% CO in the reformate. Theoretically, this could be converted into hydrogen and carbon dioxide with an additional water gas shift reaction resulting in a 50% hydrogen yield. They also found that the best results came by preheating the diesel so that it entered the Plasmatron as vapor.

The intention of the design is to be used in conjunction with an existing engine, such as in an automobile. A concept of the system is shown in Figure 1-7.
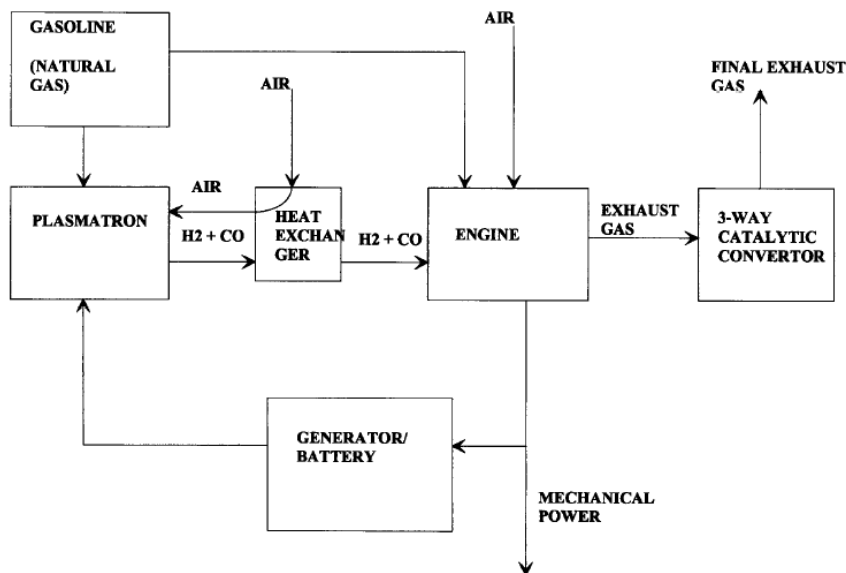
Figure 1-7: System concept of Plasmatron use with an engine [33].

A very rich air-fuel mixture would feed into the Plasmatron to produce syngas. This hydrogen-rich fuel would then combine with unreformed fuel and secondary air to create a lean mixture for injection into the engine. The lean operation of the engine would significantly lower combustion temperatures, potentially lowering NOx emissions by a factor of 100. A portion of the chemical energy of the fuel is released during the reforming process, and the Plasmatron consumes energy during operation, but it is believed that the increased engine efficiency will offset these losses.

1.2.3 Gliding Arc Plasma Reactor

Research by Lesueur et. al. [34] and Paulmier et al. [29] investigated the use of a gliding arc plasma to reform gasoline fuel. The gliding arc principle is thought to be invented by Albin Czernichowski [2], but it has been used by many researchers across the world. The principle consists of diverging electrodes with gas flowing from the bottom of the electrodes as shown in Figure 1-8.
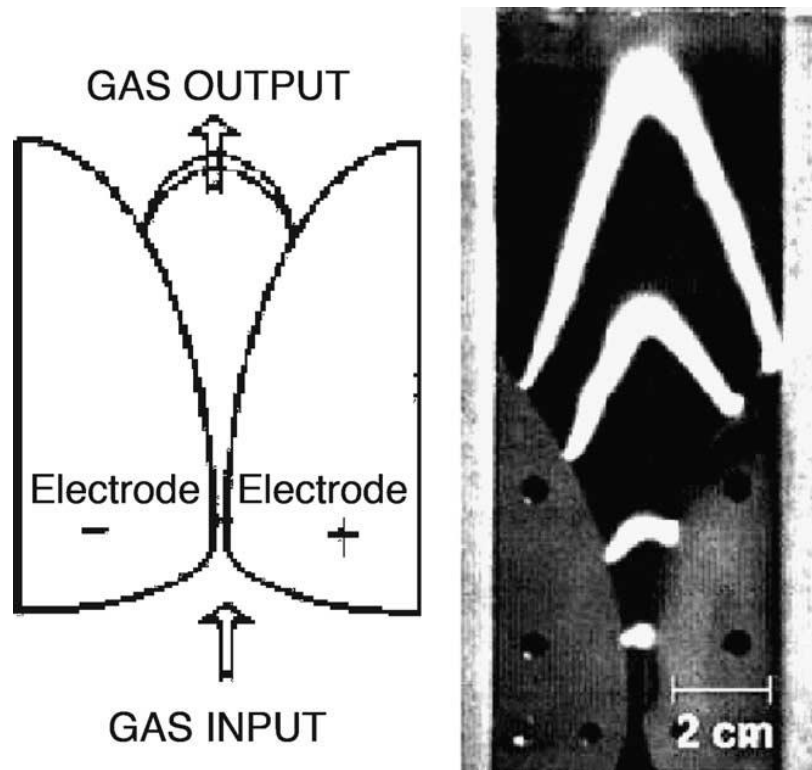
Figure 1-8: Gliding arc plasma [29].

When a high voltage is applied between these electrodes, an arc is formed at the bottom where the distance between the electrodes is smallest. The injected gas pushes the arc upwards, increasing the length of the arc. When the arc reaches the top of the electrodes, the arc re-establishes at the bottom of the electrodes. This particular plasma reformer [29] is designed to use an auto-thermal reforming process, which combines the steam reforming and partial oxidation processes. It was also constructed to operate at pressures up to 3×10^5 Pa which is significantly higher than most reformers. The plasma reactor uses two gliding arc systems in series to treat a larger volume of fuel. The electrodes are powered by a high-voltage power supply that creates potential differences of 5000 and 10,000 Volts (AC or DC) respectively for

the two sets of electrodes. Power consumption of the reactor reached 1000 W. Gasoline was vaporized and mixed with air and water to be treated.

Best results from the plasma reactor came under steam reforming conditions with a yield of 30% H_2 and 17% CO. Again, with the assumption that a water gas shift reaction will take place, this leads to a hydrogen yield of 47%. It was noted that the efficiency of the reformer decreases as the fuel flow rate (velocity) is increased, owing to decreased residence time of the fuel. Consequently, it was shown that increasing the pressure of the reactor increases the efficiency because this increases the residence time of the fuel [29].

1.2.4 Plasma Assisted Combustion

Aside from syngas production, plasma can be used to add energy to the combustion process [23-27] to create radicals as mentioned previously. Work performed by B.F.W. Vermeltfoort [35] investigated plasma assisted combustion where the aim of the plasma was not necessarily to produce syngas. A low-swirl burner was used with a non-thermal plasma under lean conditions in order to reduce NOx emissions by lowering the flame temperature. Chain branching reactions during combustion are responsible for creating radicals and free atoms that are essential to energy release. In this case, plasma was used to create even more highly energetic radicals that enhance the combustion process even further. It was also shown that initiating a chain reaction by other means than heat can be much more efficient, which in this case means initiating chain reactions with plasma.

A low-swirl burner was used to create turbulent mixing of a methane-air mixture for combustion. This type of burner was already shown to perform well with lean mixtures, but was

modified with a non-thermal plasma application to investigate the effects of plasma assisted combustion. Preliminary testing used a ring-pin setup for plasma application, but this setup showed poor results, most likely due to a short residence time between the mixture and the plasma. A new design was incorporated, consisting of a coaxial pin anode surrounded by a mesh wire cathode wrapped around a quartz tube. With the quartz tube located between the pin and mesh, a dielectric barrier discharge (DBD) was formed. The fuel mixture flows inside the tube, allowing a volumetric plasma to interact with it.

The main goals of this particular research were to investigate the blow-off limit of propane and methane mixtures with plasma assistance and to monitor the emissions of the flame. The blow-off limit refers to the point at which the mixture becomes too lean to combust. It was shown that the use of the DBD plasma did improve the blow-off limit. However, the plasma also caused NOx emissions to increase, which was not desirable.

1.3   Research Objectives

The first objective of the present research was to characterize the plasma generator supplied by Clean Diesel LLC to determine its plasma properties and its abilities to perform under desired burner conditions. It was characterized by analyzing the voltage and current characteristics of the plasma under the expected operating conditions. The plasma was then analyzed through optical emission spectroscopy in terms of its type and its parameters such as temperature and electron number density (this task was necessary to compare it with other plasma reformer setups). The plasma generator is a unique invention and was the focal point of the project. The ability to make changes and adjustments to the generator was quite limited, and

19

the ability to have it repaired was difficult because only the inventor has in-depth knowledge of its construction. For these reasons, the plasma generator was used only as specified by Clean Diesel LLC, and any improvements were made to other system components.

The plasma characterization effort was in support of the investigation of fuel reforming capabilities of the plasma generator to increase combustion efficiency and reduce emissions. The plasma was used for combustion purposes in a modified oil burner, where performance results were compared to that of a stock burner (of the same type). The oil burners were tested in a hot water heating system to simulate a real-life application for the invention. This aspect was important to Clean Diesel; large investments have been made for this invention to be commercialized for home-heating applications. The overall goal of the oil burner testing was to show that the assistance of plasma to the combustion process showed improvements in performance that outweighed the additional power consumption of the plasma generator. Specifically, we were looking for improvements in the thermal efficiency that allowed for decreased fuel consumption and reductions of harmful combustion products such as carbon monoxide, nitrogen oxides, and particulate matter.

Chapter 2

Plasma Generator Characterization

The plasma source used in all the work for this thesis was provided by Clean Diesel LLC. The invention was patented in 2005 under the title "Furnace Using Plasma Ignition System For Hydrocarbon Combustion" [36]. The plasma generator was designed for application in internal combustion engines or for fuel burners in a furnace. The patent includes descriptions of the electrode placement for use in the fuel burner, and it also provides details on the electrical circuitry of the plasma.

2.1   Plasma Generator

Physically, the plasma generator is housed in a white box that measures approximately 30 x 70 x 50 cm and weighs around 35 kg. Its frame is made of a non-conducting material that can be disassembled for maintenance. It includes an entrance hole for a cooling fan, as well as an exit hole on the opposite side of it. On the top of the generator are 6 threaded bolts that protrude from inside the box that are arranged in a circular fashion. These are the electrode connections for the plasma discharge. Also on top of the box is a toggle switch for the generator's power, an AC plug with a one meter cable, three toggle switches that operate the generator, two frequency-adjusting terminals, and a series of fuses. The six-electrode configuration is one of the defining characteristics of this particular plasma generator that separates it from other designs. The

intention of this design was to create a spatially uniform volume of plasma that would effectively interact with a hydrocarbon fuel. This method differs from that of typical fuel burner ignition techniques, where an ignition spark is provided on only one side of the fuel spray. The plasma generator is shown in Figure 2-1.

Figure 2-1: Plasma Generator.

The current version of the plasma generator runs on 120 VAC from a standard wall outlet for its use in fuel burners. This provides an easy and reliable power supply to access. Within the generator, a power converter converts the 120 VAC into 24 VDC. The DC power is subsequently transformed into a higher voltage for the electrode discharge by transformers. A component of the plasma generator is a signal generator that creates a square wave that is divided into 6 sequential lines for the 6 electrodes. The original square wave signal operates between 0 to 5 Volts and between 5 and 30 kHz. The circuit utilizes a signal overlap circuit to overlap the sequential signals. The signals from the six lines then go through a signal driver where the signal

22

is sent out through six transmission lines. Diagrams of the signal generator are shown in Figure 2-2 and Figure 2-3.
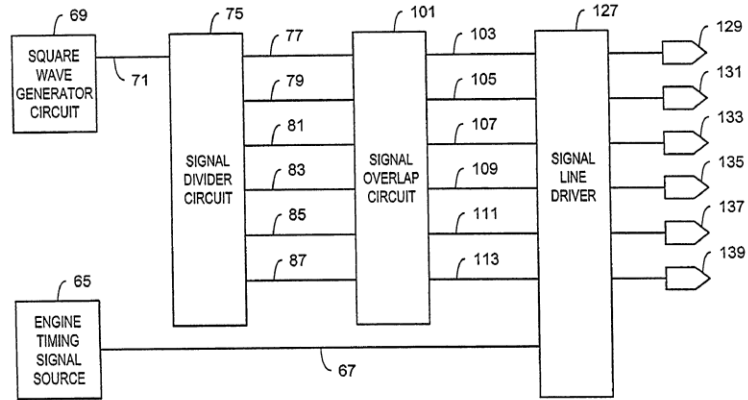
Figure 2-2: Schematic of the signal generator.
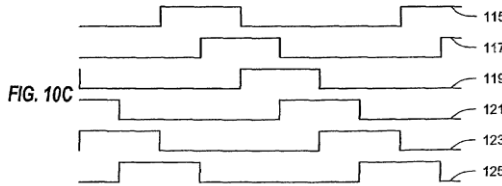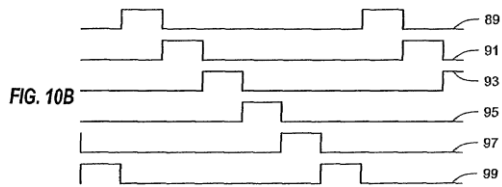
Figure 2-3: Schematic of the signal produced by the signal generator.

Figure 2-2 shows the schematic of the signal generator where a 5V square wave is divided into six lines, and then the lines are overlapped. Figure 2-3 shows what the individual signals look like as a generic function of time. The original square wave is created (FIG. 10A), then divided (FIG. 10B), then overlapped (FIG. 10C). Note that the Engine Timing Signal Source is not utilized in these experiments. From the signal generator circuit, each sequential square wave is transmitted to its own power MOSFET. The discharge circuit includes six lines that are connected to the 24 VDC power supply. A MOSFET is located on each of these circuits with the intention of opening or closing the primary side of the voltage transformer. When the square wave is received by the MOSFET, it closes the circuit loop for the 24 VDC power supply, thereby allowing current to flow. The current goes through the primary winding of a high voltage automotive transformer; the secondary winding produces a high voltage that is sent to the discharge electrodes. A schematic of a single MOSFET/Transformer circuit is shown in Figure 2-4.
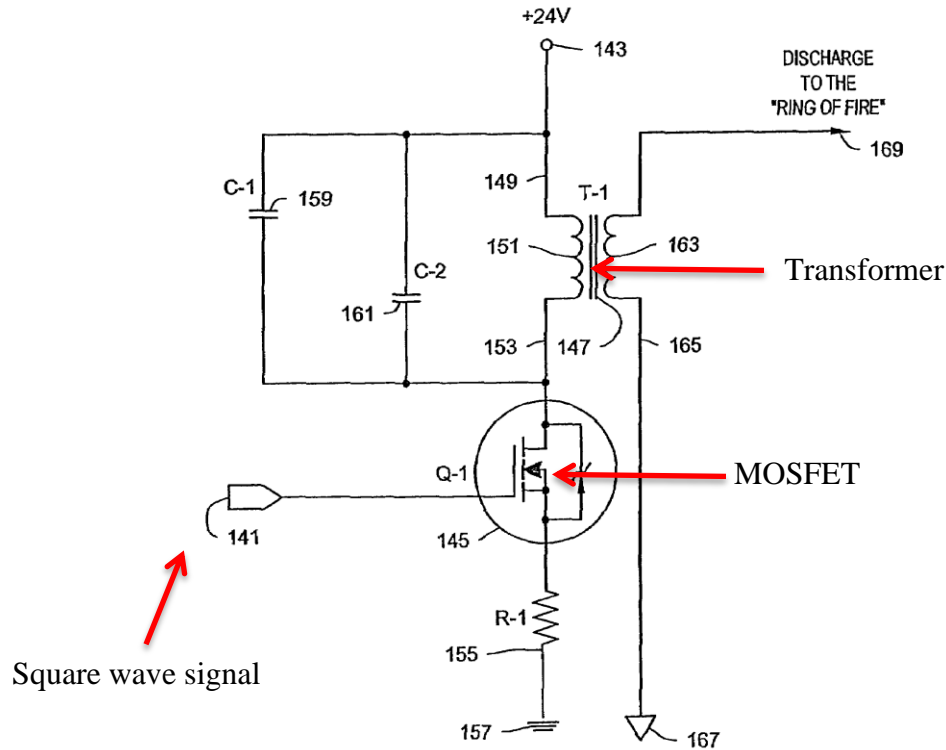
Figure 2-4: Schematic of single MOSFET/Transformer circuit.

All six lines on the primary winding side are connected to the earth ground as connected to the ground receptacle on the external AC plug. However, the secondary windings share the same floating ground with each other, which is not necessarily the earth ground. This circuitry creates a complex discharge system where electrodes are discharging sequentially to other electrodes that connect to the same floating ground and it produces a volumetric plasma between the six electrodes. To the human eye, the resulting plasma appears as a stationary hemispherical ball of light as shown in Figure 2-5. The plasma also emits an audible high-pitched tone during its operation. The plasma uses copper wire for its six electrodes in this picture, and the white tube under the plasma is for air flow which will be explained later.
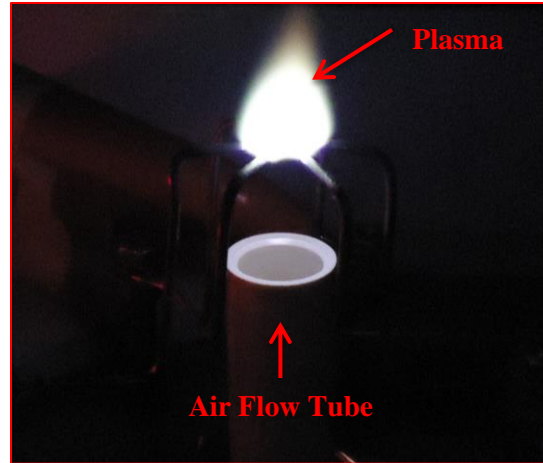
Figure 2-5: Image of plasma formed by the plasma generator.

Figure 2-5 shows electrodes made from bare 14 AWG copper wire that were used for the plasma characterization testing, while Riello burner electrodes were used for burner testing. The use of the copper electrodes allowed for the plasma to be created right on top of the plasma generator, which was both simple and effective. The electrode distance was kept between 8 and 15 millimeters for all testing. The electrode distance refers to the point-to-point distance between opposite electrodes, not adjacent electrodes. This distance was utilized because the existing electrode assembly provided by Clean Diesel utilized an electrode distance in this range. Extending the distance has the potential of damaging the plasma generator, as a higher voltage would be required to maintain the plasma at larger distances (this could result in a higher power dissipation within the transformer resulting in eventual damage).

The plasma created by the plasma generator appears visually stable, as mentioned before, but it is very sensitive to disturbances of its medium. All characterization testing with the generator utilized air as its medium, meaning nearly all of the ionization occurs with oxygen and nitrogen molecules. Disruption of the plasma occurred easily by simply blowing or breathing across the plasma. Its shape was distorted and pushed in the direction of the flow, and even the

noise it produces sounded disturbed. To better understand the formation of the plasma and the effect of flow disturbances, images were collected with an Intensified Charge-Coupled Device (ICCD) camera. This camera provided the means necessary to detect light with very small exposure time to visually assess the plasma that is impossible to do with the human eye. Figure 2-5 shows the plasma operating in a stationary air (no flow) condition with a 500 ns exposure time.
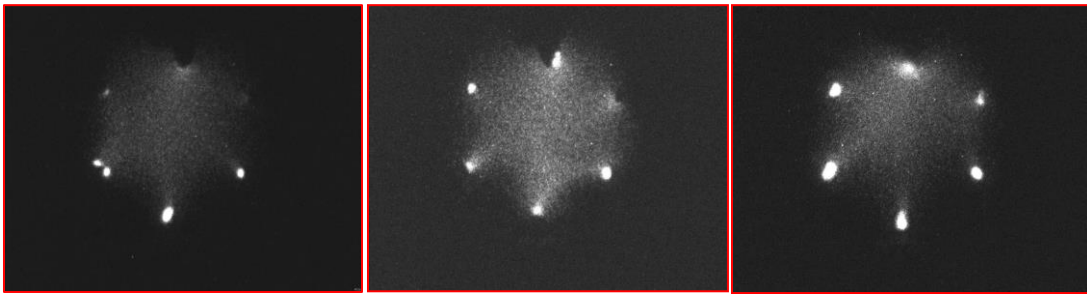
Figure 2-6: ICCD images of plasma under 1 kHz and stationary air conditions.

Electrical discharges are seen in these images as the diffused light between electrodes. Note that the variances of the images are due to differences in the discharge time. The plasma is shown strongly near the heated electrode tips and in the bright regions that span between electrodes. The plasma is shown spanning gaps across the central region of the configuration, which explains why it appears as a uniform volume. Figure 2-7 shows the plasma with the addition of an axial air flow.
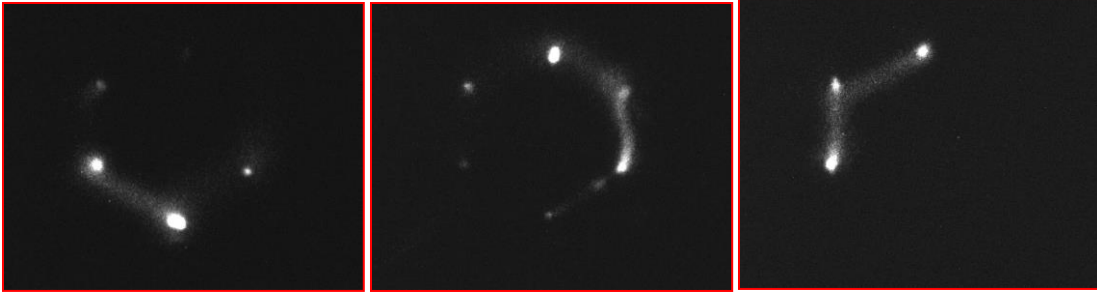
Figure 2-7: ICCD images of plasma subject to axial air flow.

These images, collected with the same exposure time as the others, show that the addition of flow to the plasma causes it to lose its volumetric form. Plasma does not form across the central electrode gap and instead is shown discharging to neighboring electrodes. The shorter path through the medium is less resistive to current flow than the path to electrodes that are further away. This effect is magnified by the air flow because the molecules that transfer electrons are now being pushed away from the electrodes. This situation will occur in the fuel burner application because of strong air flow perturbations in the burner.

2.2 Electrical Measurements

Electrical measurements of the plasma generator are needed to determine its power consumption, as well as the electrical parameters that define the plasma. The plasma generator was designed for increasing efficiencies of combustion systems by producing more energy from the same amount of fuel or by producing the same energy by utilizing less fuel; the goal being that utilizing the plasma generator should show benefits in energy production that outweigh the additional energy consumed by the plasma generator. In addition, the voltage and current that the

discharge utilizes will help determine what type of plasma it is, as well as additional parameters that can further characterize the plasma such as the electrical field strength.

The plasma generator has the ability to change the frequency of the signal generator with an adjusting screw on top of the generator. This adjustment was utilized during testing to determine its effect on the plasma's behavior. The patent for the generator states that the frequency generator is variable and is assumed to represent the frequency of the original square-wave before it is divided into six transmission lines. For our electrical measurement tests, the frequency is referred to as the frequency of individual pulse discharges. In other words, the frequency of the plasma describes the rate at which any MOSFET allows a discharge through its electrode. The majority of the burner testing utilizes a frequency of 1 kHz, but 2 and 3 kHz frequencies were also utilized, especially for characterizing the plasma.

To create the plasma for the electrical measurements, copper wires were used as the electrodes. The wires were attached to the electrode bolts on the generator and used to form a ring-shape with an electrode distance of 10.6 mm as shown in Figure 2-8.
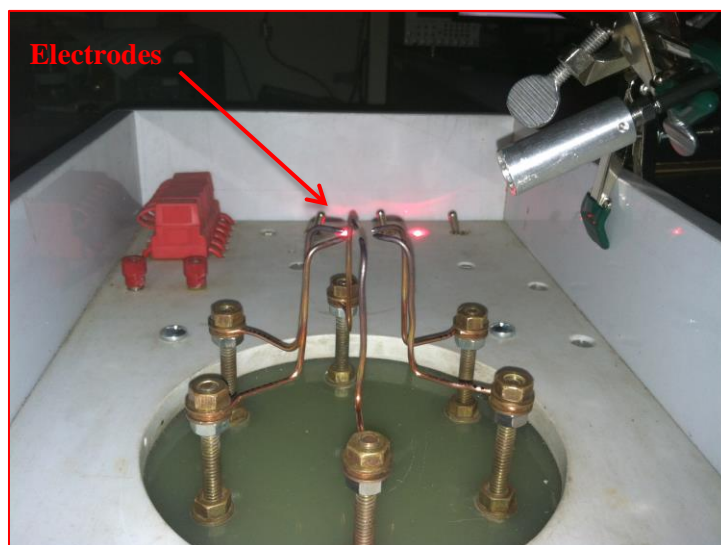
Figure 2-8: Electrode setup with copper electrodes.

29

Power consumption of the plasma generator was measured with a wattmeter (Kill-A-Watt Meter) provided by Clean Diesel. It was not the most effective nor accurate device to measure the exact power consumption, but for reasons that will become obvious in future chapters, the wattmeter was adequate for approximate data. Power consumption was measured for the plasma generator operating at 1, 2, and 3 kHz in stationary air conditions and is shown in Table 2-1. Again, note that these values are approximations, as the meter's reading fluctuated by close to 5% of the average value.

Table 2-1: Power consumption of plasma generator at 1, 2, and 3 kHz.

Generator Frequency	1 kHz	2 kHz	3 kHz
Total Power Consumption	560 W	525 W	490 W
Plasma Consumption	404 W	369 W	334 W

Of the total power consumption shown in Table 2-1, 156 W is consumed by the cooling fan alone. This aspect of the system could be constructed more efficiently in the future, so it can be subtracted to determine the power consumption of the plasma generation. To measure the voltage and current characteristics of the generator, a 600 MHz oscilloscope (Lecroy Waverunner 64Xi) was used in conjunction with a 1000X (attenuation) high voltage probe (BK Precision PR-55) and current clamp probe (Fluke 80i-110s). The equipment was set up as shown in Figure 2-9.
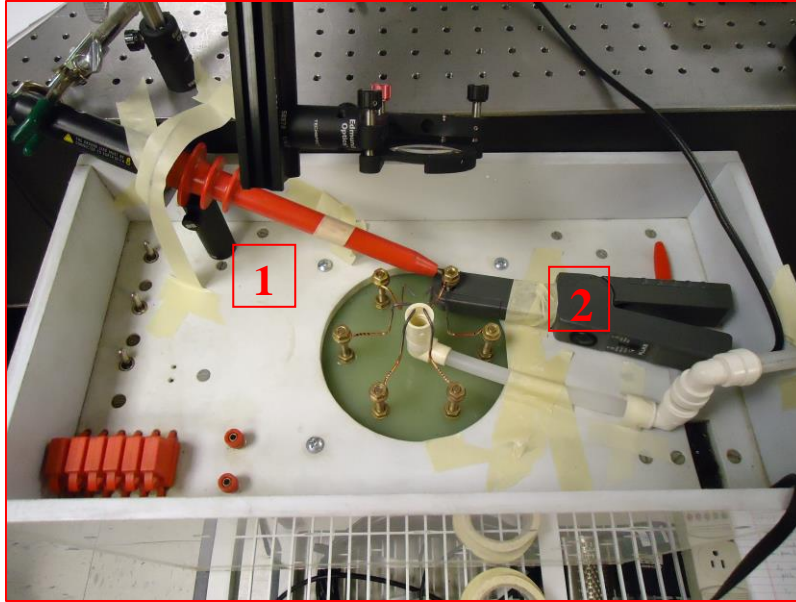
Figure 2-9: Experimental setup for voltage/current measurements. 1) High Voltage Probe, 2) Current Clamp.

The voltage probe was placed on one of the six electrodes and measured the voltage with respect to earth ground. The current clamp was located on the same electrode and both probes connected to the oscilloscope. The white tube located under the plasma region was used to add air flow to the plasma. A cylinder of air with 1% H_2 was used and controlled by a rotameter. Data from the oscilloscope is shown in Figure 2-10 with the plasma generator operating at 1 kHz with no air flow (and no added H_2).
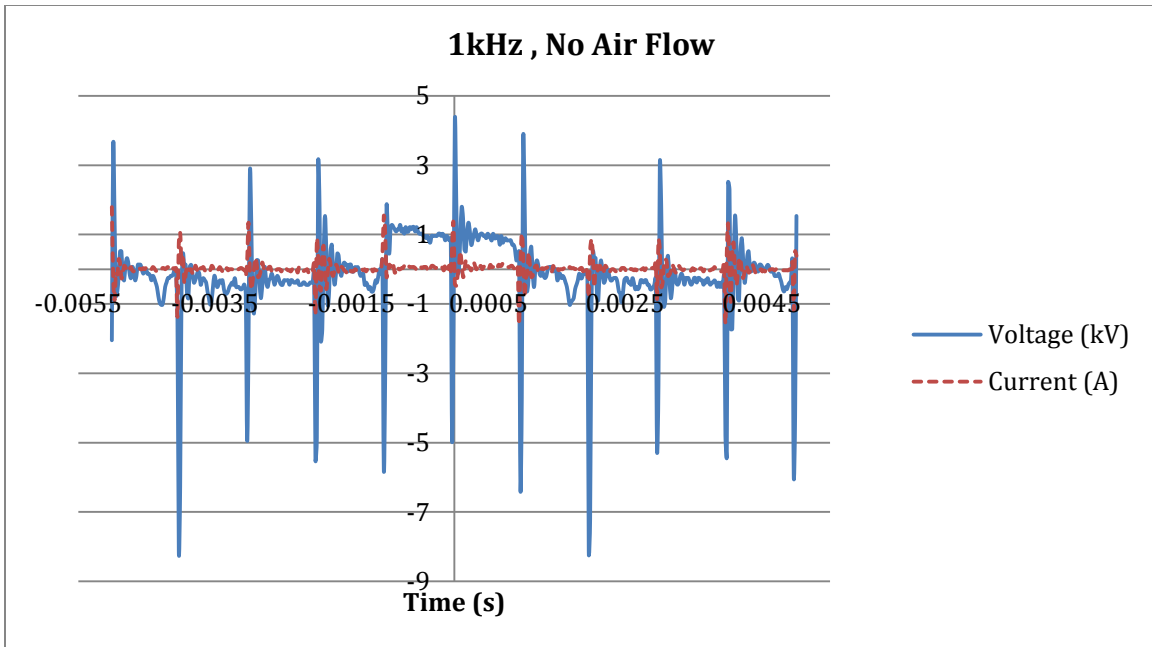
1kHz , No Air Flow

Figure 2-10: Voltage and current measurements of plasma at 1 kHz and no air flow.

The waveform of the voltage and current data is complex. The voltage waveform shows the potential difference of the electrode with earth ground, but the desired voltage is the potential difference between the electrode and its floating ground (which could not be readily measured). The spikes in the voltage and current curves are representative of plasma discharges where a breakdown voltage is achieved which allows for current flow. The alternating nature of the curves may be attributed to possible ringing or resonance phenomena from different resonating capacitors included on the primary side of the circuit.

With the addition of approximately 9 LPM of air flow to the plasma, the voltage and current relationship is shown in Figure 2-11, once again at 1 kHz.
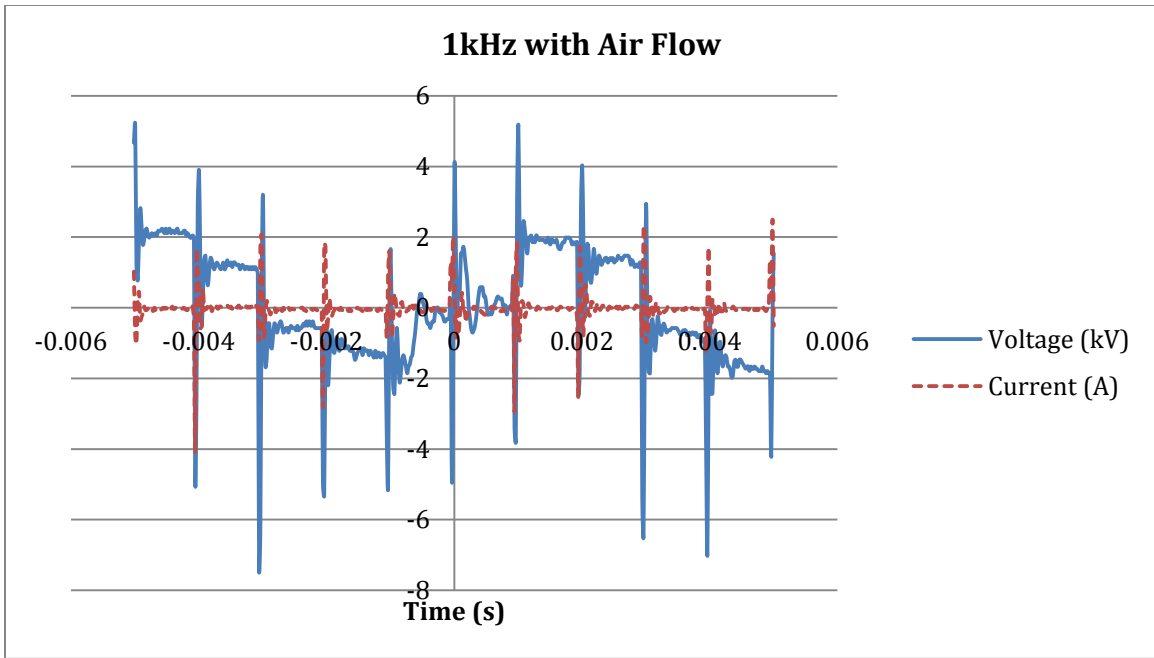
Figure 2-11: Voltage and current measurements of plasma at 1 kHz with air flow.

This plot is similar to the plot with no air flow, but the voltage seems to vary further away from zero in between spikes (which presently cannot be explained). Unfortunately, this does little to help understand the altering of the plasma formation. The difference in the plots between 1, 2, and 3 kHz frequencies are as to be expected with the same plot shapes with different periods as shown in Figure 2-12.
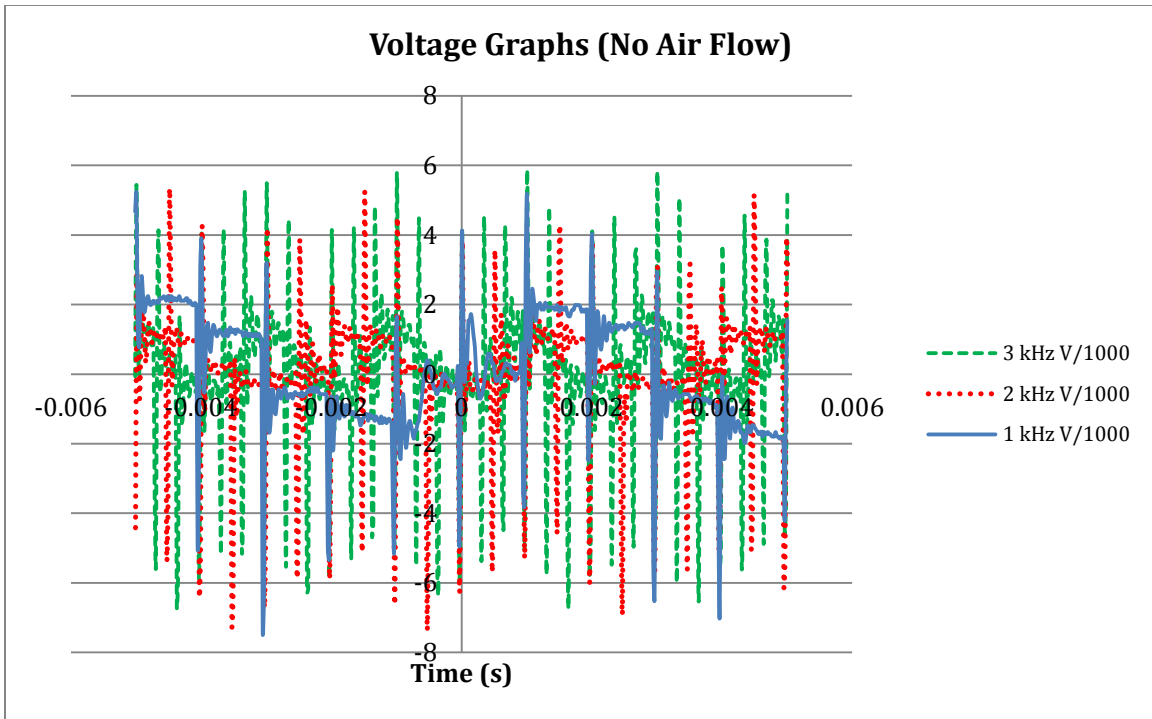
Figure 2-12: Voltage and current measurements of plasma at 1, 2, and 3 kHz and no air flow.

It was strongly desired to determine the electric field of the plasma, but the interconnecting electrodes made this task challenging. In summary, the electrical characterization did provide details on the power consumption and the circuit analysis of the plasma generator. The plasma generator creates high voltage DC discharges through electrodes that discharge to other electrodes that act as a floating ground. The peak voltage values tend to measure 4-6 kV with respect to earth ground, and the peak current tends to be between 1-2 A. The electrodes discharge sequentially in a rotating fashion at a rate that appears to make a continuous plasma in the circular region between the electrode tips.

Chapter 3

Optical Emission Spectroscopy of Plasma

Optical emission spectroscopy (OES) is a widely used technique for plasma characterization due to its non-intrusive nature and simple data collection. The goal of OES in this project was to characterize the plasma created by the plasma generator and better understand its operating regime and suitability for fuel reforming purposes. The main parameters of interest were the electron number density, electron temperature, vibrational temperature, and rotational temperature.

3.1   Experimental Setup

The system used to perform the spectroscopy on the plasma generator was located in the Engineering Research Center at Colorado State University's Foothills Campus. The spectrometer used was a Princeton Instruments Spectra Pro 2750 which was connected to a CCD (Charged-Coupled Device) collector. The entrance slit width determined the amount of light collected, and a chosen grating determined the resolution and range of the collected spectra. The grating is characterized by its grooves per millimeter (lines/mm) rating and blaze angle. The blaze angle affects the efficiency of the grating at reflecting certain wavelengths, meaning certain gratings have blaze angles that are better suited for a specific wavelength range. For our system, the first step was to determine the instrumental broadening of spectral lines for different entrance slit

widths of the spectrometer by using a Hg-Ar lamp. The following section describes the acquisition procedure, instrumental broadening measurements, and the optical system used to collect spectra from the plasma generator.

3.1.1   Acquisition of Spectra

The general procedure for collecting spectra started with the setup of the spectrometer and its software, Winspec/32. The entrance slit width was adjusted to the desired width with a micrometer. A large core, multi-mode fiber optic cable was connected to the entrance slit, while its opposite end was set up to collect light from the source. The spectrometer had three available gratings (150 g/mm, 1200 g/mm, and 3600 g/mm where g/mm is grooves per millimeter) which were selected based on the wavelength being examined, and the resolution desired. The grating and the center wavelength for collection were selected through the software. Next, the exposure time was set to collect enough light to capture an image but prevent over-exposure from too much light. Before collecting spectra from the light source, a background image was first collected, which can then be subtracted by subsequent images to eliminate unwanted light from the spectra. More details on the optical system for plasma measurements are provided in Section 3.1.3. Once an image was collected, the image was analyzed to determine exact wavelengths and corresponding intensities. A Matlab code was developed to convert an image, such as the one shown in Figure 3-1, into a quantitative spectrum as shown in Figure 3-2.

Figure 3-1: Spectrum collected with 150 g/mm grating, 10 micron slit width, and 5 ms exposure time.
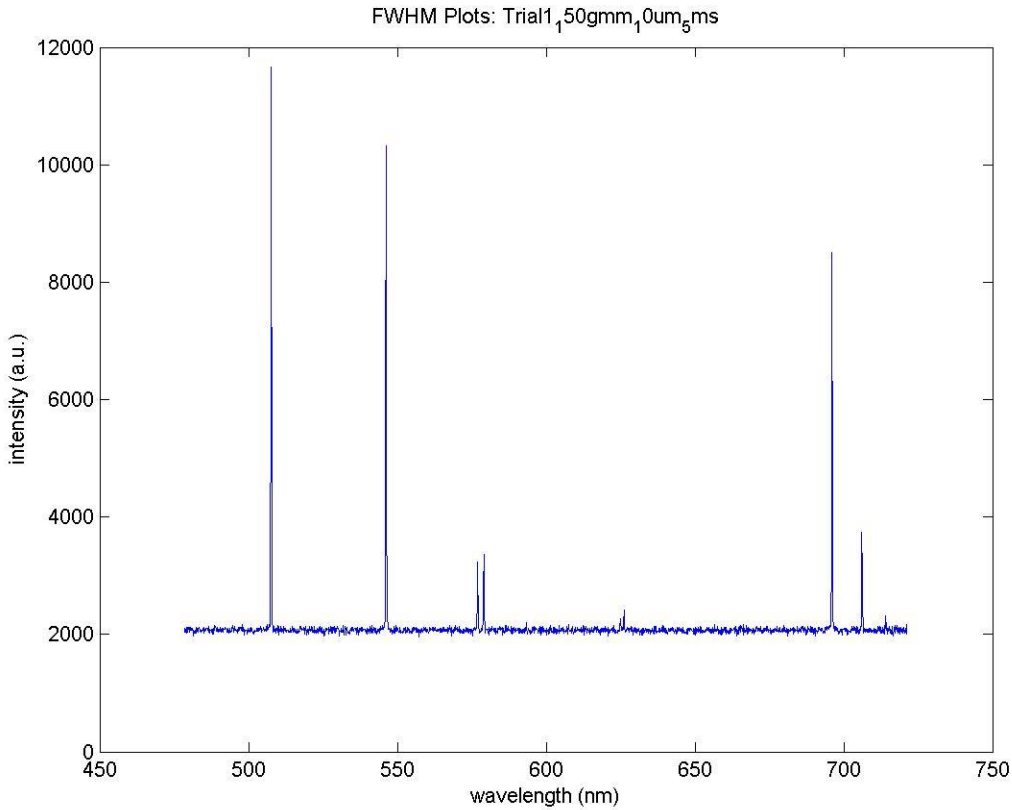
Figure 3-2: Spectrum corresponding to image of Figure 3-1.

The MatLab code converted the image collected by the Spectra Pro software into a plot of intensity vs. wavelength by using wavelength calibration curves (specific to the center

wavelength and grating used). It should be noted that a relative intensity calibration of the spectrometer was not performed to account for detector response at different wavelengths. As will be shown shortly, the spectra most affected by line intensity were collected over very narrow wavelength ranges (~7 nm). Due to this, it was decided that the intensities of the peaks in this range would likely be unaffected by detector response.

The overall data collection procedure began by determining the instrumental broadening of the spectrometer. This provided values that would be utilized later to use line broadening to determine temperatures, but also helped to select the entrance slit width for data collection. As for the plasma spectra, multiple conditions were examined. The effect of the plasma generator frequency was investigated, as well as the effect of air flow through the plasma. Plasma frequencies of 1, 2, and 3 kHz were used under conditions of no air flow and a flow of air with 1% H_2 at approximately 9 liters per minute (LPM). This flow rate was chosen because it was low enough to prevent total disruption of the plasma, but high enough to notice an effect. The air flow was controlled by a Gilmont Accual GF4340 flow meter connected to a cylinder of air with 1% H_2. The air flow exited a PVC elbow located directly below the plasma as was shown in Figure 2-5. This testing layout provides spectra under six different conditions that were compared to SPECAIR calculations to determine plasma parameters.

3.1.2 Instrumental Broadening Versus Slit Width

The next step taken in the spectroscopic analysis of the plasma was to determine the ideal slit width to use for testing. This was done with a Mikropack Cal-2000 Hg-Ar lamp. The fiber optic cable was connected from the spectrometer to a port on the light source. Two spectral lines

were the focus of this procedure, at 365 and 546 nanometers. The 150 and 1200 g/mm gratings were used for the 546 nm line, while the 1200 and 3600 g/mm gratings were used for the 365 nm line. The slit widths used were 10, 20, 40, 60, and 80 microns. Slit widths of 100, 120 and 140 microns were additionally utilized for the 3600 g/mm grating. The exposure time was adjusted for each test to produce a sharp image for each setup. Each image was then analyzed with the MatLab code to produce a plot similar to Figure 3-2. The plot was then further analyzed with PeakFit software to determine the FWHM of the 365 and 546 nm spectral lines. Voigt profiles were used for these calculations.

The next step in this process was to compute FWHM's for the same lines (based on spectrometer parameters and neglecting other broadening mechanisms) to compare to the experimental results. Equations 3.1-3.3 were used to determine the theoretical FWHM for the spectral lines:

$$FWHM = W \; x \; R_D \hspace{3cm} (3.1)$$

$$R_D = \frac{1}{fd} \hspace{3cm} (3.2)$$

$$FWHM = \frac{W}{fd} \hspace{3cm} (3.3)$$

where R_D is the Reciprocal Linear Dispersion, W is the width of the entrance slit, f is the focal length of the spectrometer (750 mm), and d is groove density of the grating. The theoretical and experimental FWHM's for the two spectral lines are shown in Figure 3-3 and Figure 3-4. The data is also summarized in Table 3-1. For most cases, there is a reasonable agreement between measured and calculated values with some discrepancies at narrow (~10µm) slit widths (possibly attributed to imperfect matching of the fiber to the spectrometer).
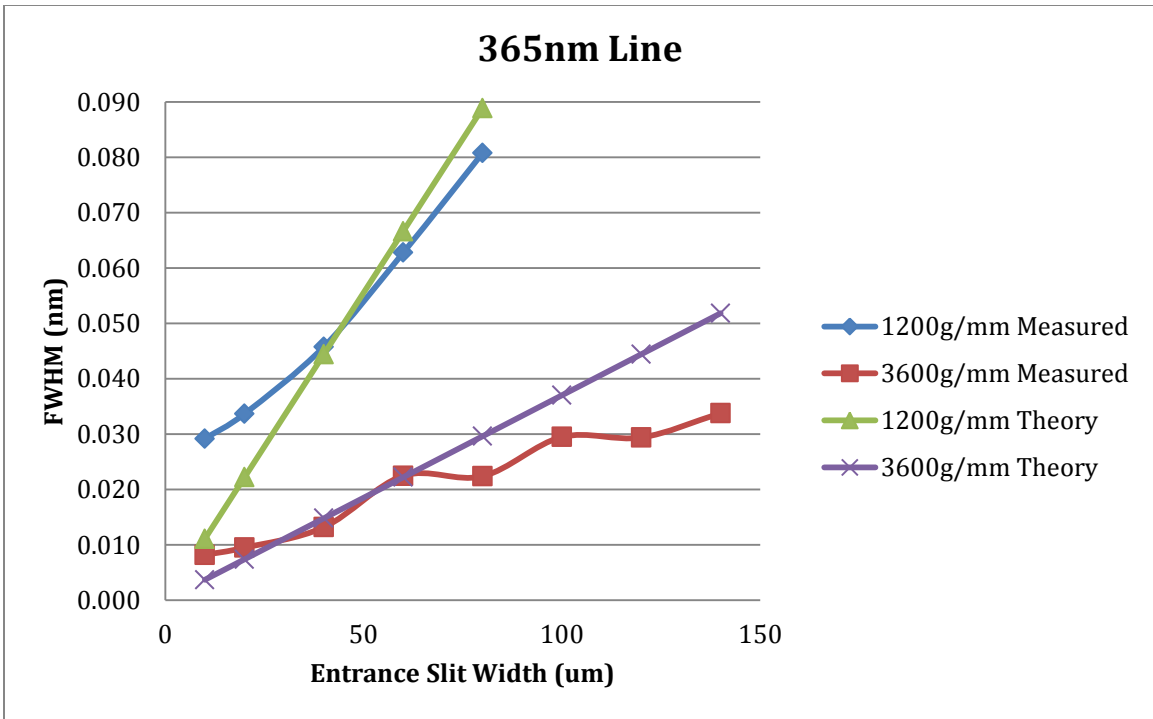
Figure 3-3: FWHM vs. Slit Width for the 365 nm line.
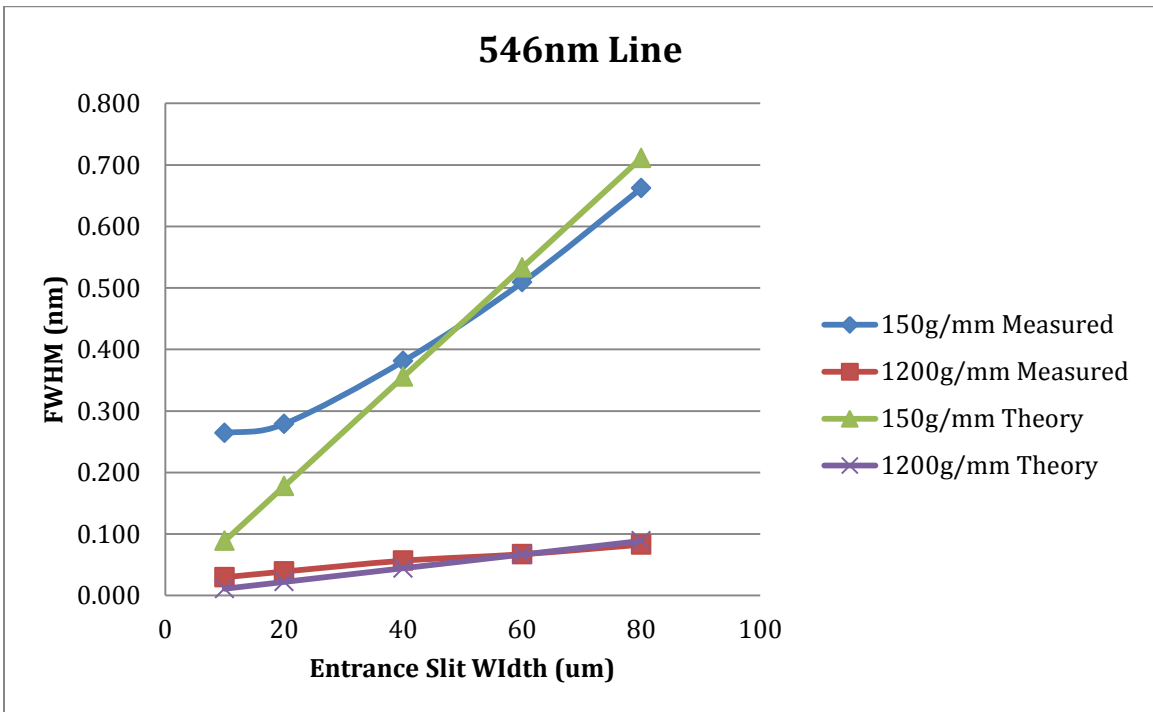
Figure 3-4: FWHM vs. Slit Width for the 546 nm line.

Table 3-1: Experimental and theoretical FWHM (in nm) of entrance slit widths.

365 nm Line				
Slit Width (um)	1200g/mm Measured	1200g/mm Theory	3600g/mm Measured	3600g/mm Theory
10	0.029	0.011	0.008	0.004
20	0.034	0.022	0.010	0.007
40	0.046	0.044	0.013	0.015
60	0.063	0.067	0.023	0.022
80	0.081	0.089	0.022	0.030
100			0.030	0.037
120			0.029	0.044
140			0.034	0.052

546 nm Line				
Slit Width (um)	150g/mm Measured	150g/mm Theory	1200g/mm Measured	1200g/mm Theory
10	0.264	0.089	0.030	0.011
20	0.279	0.178	0.039	0.022
40	0.381	0.356	0.057	0.044
60	0.509	0.533	0.067	0.067
80	0.662	0.711	0.083	0.089

Subsequent measurements employed a 40 micron entrance slit width for which the measured instrumental broadening values closely matched theoretical calculations.

3.1.3   Optical System

An optical system was constructed to collect spectra from the plasma generator. A double-lens system was utilized for initial light collection. The first lens, located closest to the plasma, is a 5.1 cm biconvex ultraviolet-rated lens with a 100 mm focal length. The lens is mounted on a rack to which the entire optical system is mounted. The second lens, located 20.5 cm from the first, is a 2.5 cm biconvex lens with a 20 mm focal length. 15 mm from this lens, is a mount for the fiber optic cable. The distances between lenses were adjusted manually to find

the optimum setup so that the fiber optic received an ideal image. The optical rack is shown in Figure 3-5.
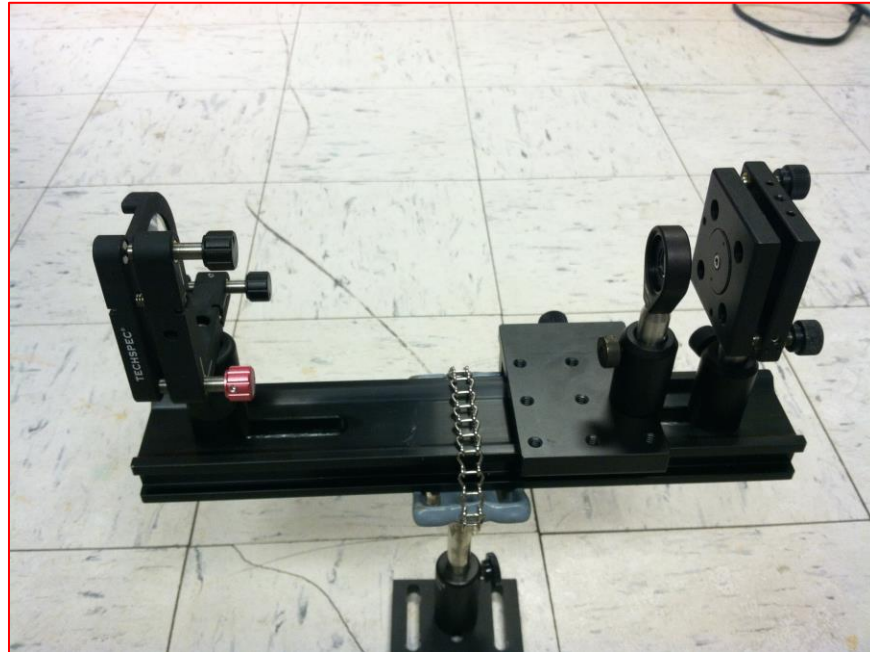
Figure 3-5: Double-lens optical rack.

The entire optical rack was mounted onto the same optics table as the spectrometer, and positioned above the plasma generator so that the first lens was 100 mm away from the center of the plasma. As with the electrical characterization portion of the generator, copper electrodes were utilized. The testing setup is shown Figure 3-6.
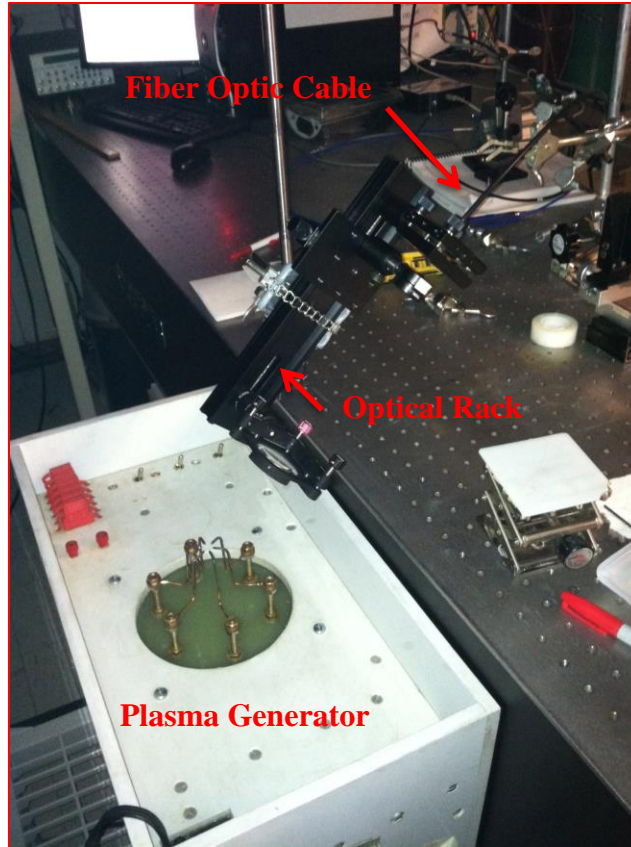
Figure 3-6: Testing setup of optical system.

3.2   Vibrational and Rotational Temperature Measurements

Optical emission spectroscopy was used to determine the vibrational (T_{vib}) and rotational (T_{rot}) temperatures of the plasma to better understand the degree of plasma non-equilibrium. Temperature measurement was performed by comparing spectra collected from the plasma generator to simulations generated by SPECAIR. By seeking agreement between reference spectra from SPECAIR with experimental spectra, vibrational and rotational temperatures were determined.

3.2.1   N$_2$ 2nd Positive System

Transitions from the second positive system of nitrogen (C-B band) were employed for determination of vibrational and rotational temperatures. This band was used as it was readily detectable and had been used in past characterizations by other researchers [4,14,18]. The transitions considered in this system all occur in the near UV region so the lenses in the optical system were rated for UV light.

Spectra were collected using all of the available gratings to provide images of the entire spectrum. Images collected with the 150 g/mm grating provided the largest spectral range, and images could be "glued" together with a glue function in the Winspec software to create a continuous spectrum over the entire range. An example of the entire spectrum of the plasma generator operating at 1 kHz and no air flow is shown in Figure 3-7.
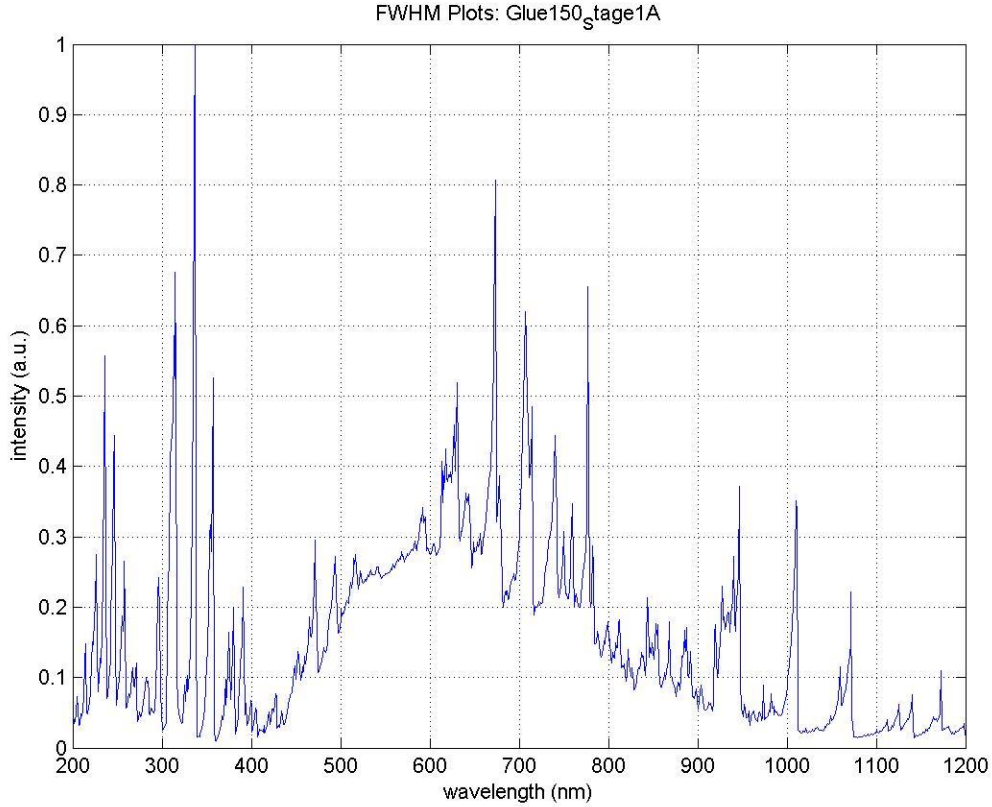
Figure 3-7: Full spectrum for plasma operating at 1 kHz and no air flow created with "Glue" function (not adjusted for detector response of relative intensity).

The spectrum of Figure 3-7 provides a general idea of the transitions that occur in the plasma. Since the relative intensities of the peaks play a large role in determining vibrational and rotational temperatures, smaller spectral ranges (over where the relative intensities are more reliable) were needed. This need led to the use of the more precise 3600 g/mm grating, which covers a range of about 7 nanometers. With multiple transitions located in this spectral range, temperatures could be found by comparing the spectra with SPECAIR simulations. The needed lines from the second positive system of nitrogen ($N_2 C^3 \Pi_u \rightarrow B^3 \Pi_g$) were effectively captured

with four images centered at 296, 334, 355, and 375 nm. These four spectra plots are shown in Figure 3-8 at 1 kHz and no air flow. The notable vibrational bands are listed in the figure.
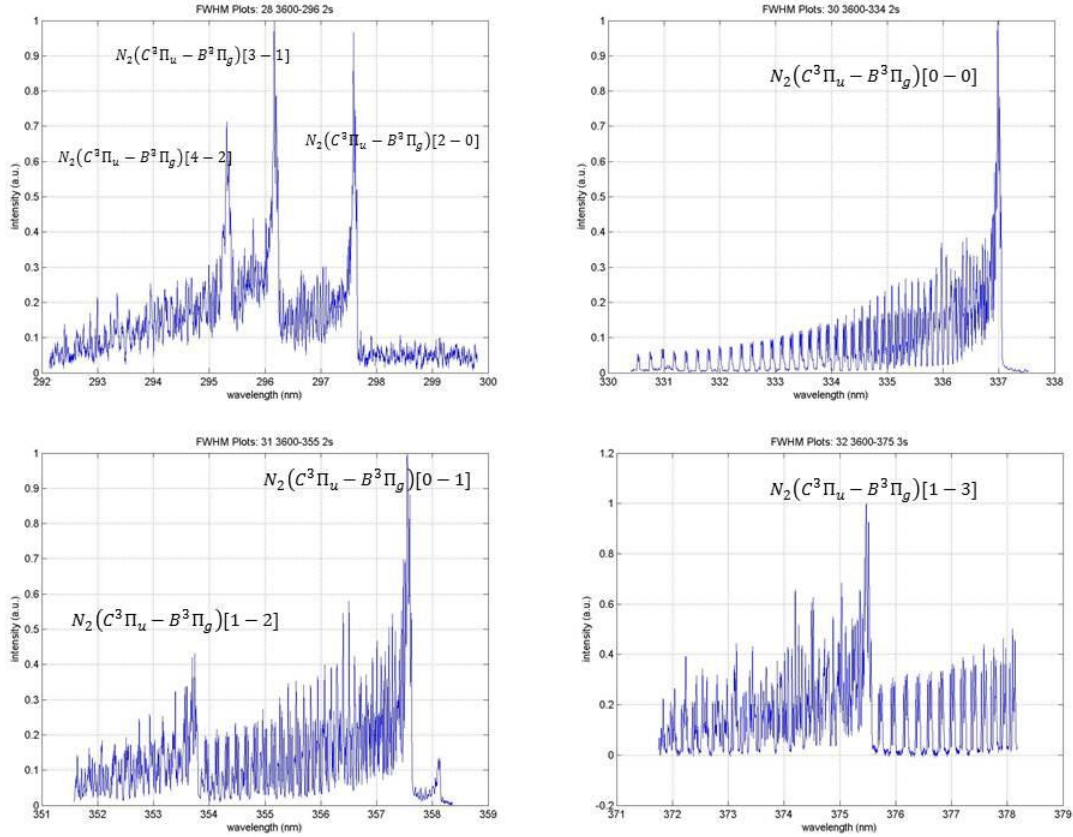
Figure 3-8: Spectra of N$_2$ (2+) transitions at 1 kHz and no air flow.

Similar spectra collected from the other five testing conditions were also collected. The notable transitions shown in Figure 3-8 are also listed in Table 3-2 with their corresponding bandhead center wavelength. In specifying the vibrational transitions, the first number represents the upper state while the second number is the lower state.

Table 3-2: Notable vibrational transitions for temperature measurements.

Wavelength (nm)	Vibrational Transition
295.2	4-2
296.1	3-1
297.5	2-0
337.0	0-0
353.6	1-2
357.6	0-1
375.4	1-3

3.2.2   SPECAIR Comparisons

SPECAIR was used to generate simulated spectra to compare with the experimental results. The simulations required a slit function to convolve with the raw spectra to generate spectra representative of those measured by the spectrometer. With an entrance slit width of 40 μm and an exit slit width of 13.6 μm (which is the pixel size), a function was developed for each grating. The function for the 3600 g/mm grating was the only one used, as only images from that grating were used with SPECAIR. The function was written as a text file and inputted into the SPECAIR program.

SPECAIR has a broad range of inputs, such as wavelength range, mole fractions of the simulation, slit function, spectral step, and considered transitions. The wavelength range was set according to the range of the experimental plot and the mole fractions used were that of atmospheric air (79% N_2 and 21% O_2). The slit function described above was used with the corresponding spectral step of 0.001 nm. The considered transition of interest for these images is the N_2 (2+) system.

The last set of inputs is for temperature, which includes electronic, vibrational, rotational, and translational temperatures. The electronic temperature is not known in our case, and was kept constant at 6000 K for all comparisons. Essentially, this input proved to have no effect on the shape of the spectra, only on the amplitude of the entire range. Since the intensities from the experimental data and the SPECAIR simulations were relative, both the experimental data and the simulations were normalized to have peak intensity equal to one. Since the rotational (T_{rot}) and translational (T_{trans}) temperatures can be considered equal [18], the number of inputs for spectral comparisons was reduced to two (T_{vib} and T_{rot}).

A trial-and-error approach was used in which the input temperatures were adjusted and resulting spectra were compared to the experimental data. Ideally, this approach would have been replaced by a computer program performing a least squares or root mean square error (RSME) fit [4] and converging on the best combination of the two inputs. However, it was discovered that the calibration curves from the spectrometer were not as accurate as needed to make such an approach reliable, as the experimental peaks were not aligning with the corresponding simulated peaks. An effort was made to manually construct new calibration curves using up to fifth-order polynomial equations, but it was decided that recalibrating all spectra would expend too much time, and this trial-and-error approach was therefore utilized instead.

As seen in Figure 3-8, two of the four spectra include only one distinguishable vibrational band. For these spectra, it was not possible to determine the vibrational temperature because there was no additional vibrational band available for comparison. However, T_{rot} was attainable in these plots with a relatively high degree of accuracy. The plots with more than one vibrational band allowed determination of vibrational temperature. Figure 3-9 shows an example of the

measured and simulated spectra near 296 nm for plasma conditions of 1 kHz frequency and no air flow. T_{vib} and T_{rot} in this case were determined to be 3600 K and 2300 K respectively.
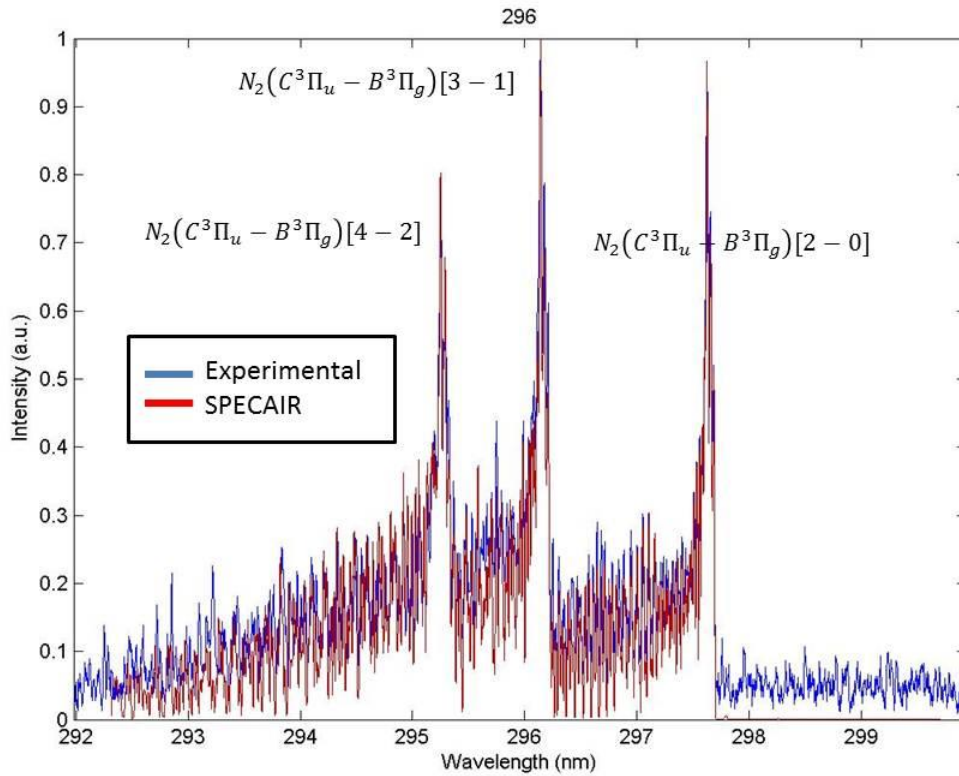
Figure 3-9: SPECAIR comparison to experimental spectrum at 1 kHz and no air flow.

The blue plot represents the experimental spectra and the red plot is the simulated spectra generated by SPECAIR. The temperatures found from each spectrum are shown in Figure 3-10 above the corresponding spectra.
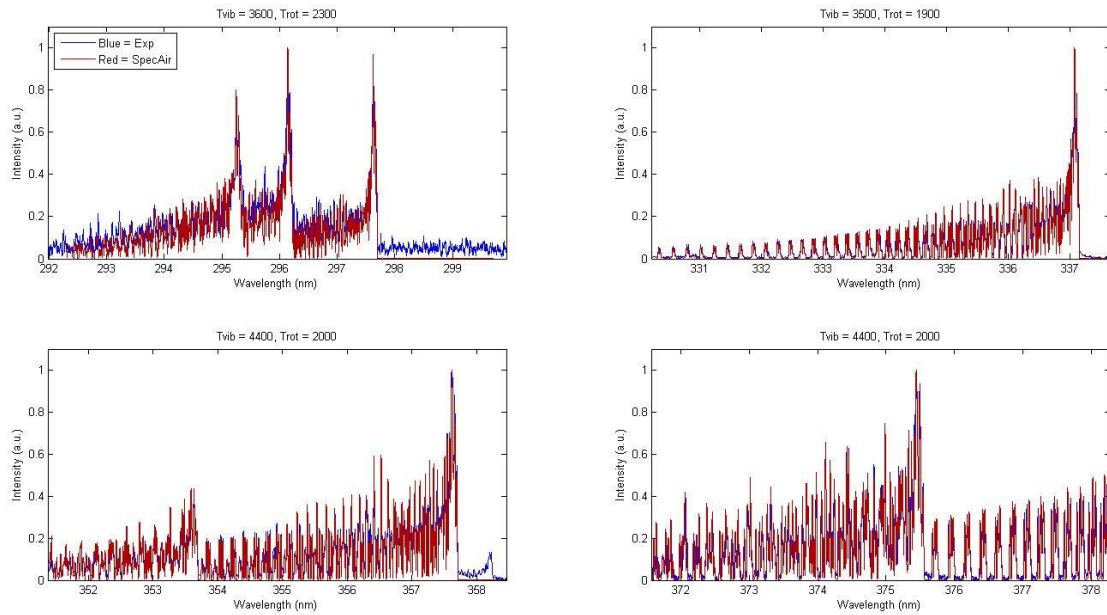
Figure 3-10: Spectra comparisons for the N_2 (2+) transitions at 1 kHz and no air flow.

The plots of the other five conditions are located in Appendix I, and the temperature data is summarized in Table 3-3. Note that the errors associated with vibrational temperatures are due to maximum excursions while the error in rotational temperatures represents the standard deviation.

Table 3-3: Vibrational and rotational temperatures of plasma at testing conditions.

Testing Condition	Spectral Region	T (vibrational) [K]	T (rotational) [K]	Avg T (vib)	+/-	Avg T (rot)	+/-
1 kHz, No Air	296	3600	2300	Avg T (vib)	+/-	Avg T (rot)	+/-
	334	-	1900	4000	400	2050	150
	355	4400	2000				
	375	-	2000				
1 kHz, With Air	296	3600	2600	Avg T (vib)	+/-	Avg T (rot)	+/-
	334	-	2000	3950	350	2125	277
	355	4300	2000				
	375	-	1900				
2 kHz, No Air	296	3600	2300	Avg T (vib)	+/-	Avg T (rot)	+/-
	334	-	1900	4000	400	1975	192
	355	4400	1900				
	375	-	1800				
2 kHz, With Air	296	3600	2300	Avg T (vib)	+/-	Avg T (rot)	+/-
	334	-	2100	4000	400	2100	122
	355	4400	2000				
	375	-	2000				
3 kHz, No Air	296	3600	2300	Avg T (vib)	+/-	Avg T (rot)	+/-
	334	-	1800	3900	300	1950	206
	355	4200	1900				
	375	-	1800				
3 kHz, With Air	296	3600	2400	Avg T (vib)	+/-	Avg T (rot)	+/-
	334	-	2000	3900	300	2100	173
	355	4200	2000				
	375	-	2000				

3.2.3 Discussion

The data in Table 3-3 reveals a large amount of information about the plasma and the accuracy of the techniques used in the data collection. It appears that the plasma frequency and the addition of air flow to the plasma have minimal effect on the vibrational and rotational temperatures as found from the second positive system of nitrogen. Next, there is disagreement in vibrational temperatures depending on the spectral range: spectra centered at 296 nm tend to yield lower temperatures than spectra at 355 nm. This discrepancy may be due to some unknown systematic error in the measurement system, or may possibly be indicative of complex vibrational distributions.

Regardless of the discrepancies in vibrational temperature, it can be concluded that the plasma generator is producing a non-thermal plasma. The non-equilibrium nature can be seen due to the different vibrational and rotational temperatures in [4], whereas a thermal plasma would show equilibrium between them. Even though the vibrational temperatures range from 3500 to 4400 K, this is still far above the nearly constant rotational temperature of approximately 2000 K.

3.3   Stark Broadening Measurements

To further characterize the plasma, the electron temperature and electron density values are necessary. These parameters can be determined from Stark broadening using the Balmer series line of hydrogen, more specifically, H_α and H_β. The original goal was to look at the H_β line at 486.1 nm, from which we could determine the electron number density by following the procedure laid out by Laux et al. [14]. However, as shown in Figure 3-11, H_β was hardly discernible from background light.
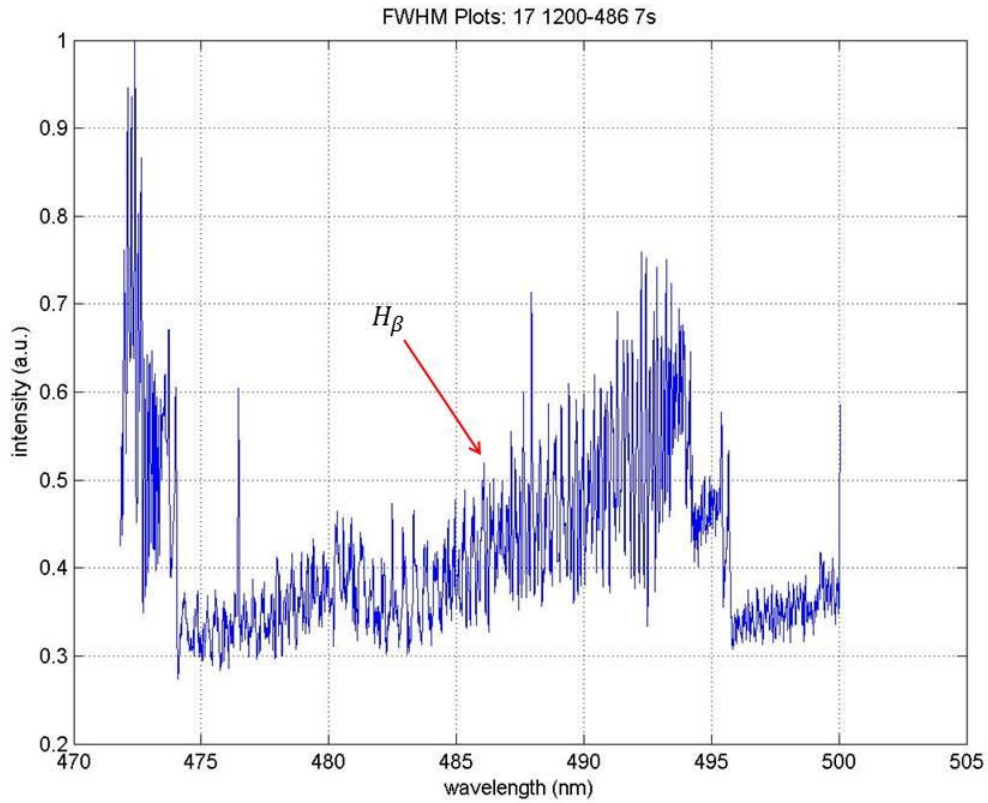
Figure 3-11: H-Beta line at 486.1 nm under 1 kHz and no air flow conditions.

Further attempts were made by measuring the broadening of the H_α line and making necessary calculations to find Stark broadening widths. The measured H_α line is shown in Figure 3-12 at conditions of 1 kHz and no air flow.
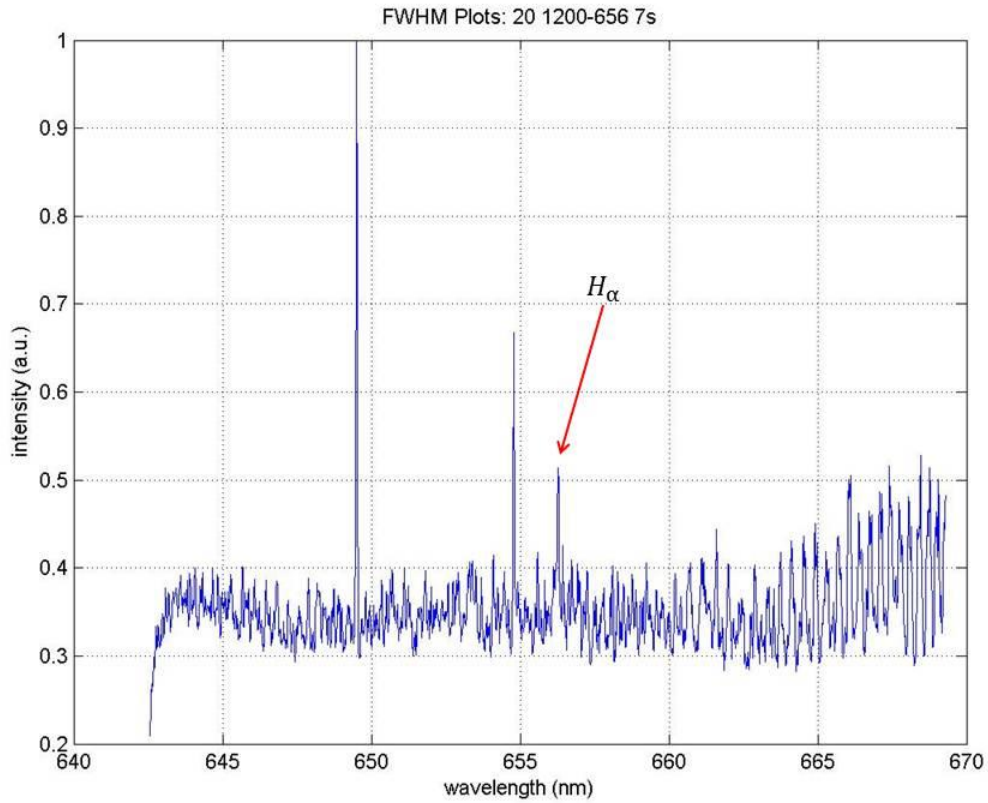
Figure 3-12: H Alpha line at 656.3 nm at 1 kHz and no air flow conditions

This analysis found that the instrumental broadening (0.046 nm) made up nearly 70% of the FWHM of the collected line. The combination of the large instrumental broadening along with contributions from both the van der Waals and Doppler broadening mechanisms made it difficult to extract the Stark contribution of the line. For these reasons, along with a lack of H_β measurements, the electron temperature and electron number density were not determined through optical emission spectroscopy.

Chapter 4

Furnace Testing with Stock and Modified Burners

This chapter explains the operation and testing of oil burners to evaluate the capabilities of the plasma generator as a fuel reforming system. A stock oil burner was obtained for the purpose of establishing baseline data to compare against plasma assisted results. Clean Diesel provided a modified burner of the same type that was used with the plasma generator. A test bed was constructed in the form of a furnace and water system to provide a means of testing the burners. Analyses of thermal efficiency and emissions were used to determine the effectiveness of the modified burner.

4.1   Oil Burners

Oil burners are common appliances for home and commercial heating, especially on the east coast of the United States. They use oil-based fuels such as kerosene, #2 fuel oil, or diesel to produce heat through combustion [37]. Oil burners consist of three systems working in conjunction with each other: a fuel delivery system, an air delivery system, and an ignition system.

4.1.1 Oil Burner Operation

The oil burner has a motor that acts as a fan for the air supply and a pump for the fuel. Fuel is gravity fed into the burner, where the pump pressurizes the fuel (700-1400 kPa for Riello burners) to flow out of a fuel nozzle and into the combustion chamber (furnace). The nozzle atomizes (vaporizes) the fuel into tiny droplets to enhance combustion and is specified by its fuel consumption rate, spray angle, and spray type (hollow or solid spray). Meanwhile, air is pulled into the burner tube by the fan. The amount of air pulled into the combustion chamber is regulated by an adjustable air gate, which allows for the control of the air-fuel ratio (AFR). The fuel pump activates a hydraulic piston that opens a damper to expose the air gate. For the burners used, the air gate is opened to an air setting marked on the damper. The setting ranges from 0-8, with 0 allowing no air in, and 8 allowing the maximum amount. A turbulator is located on the furnace side of the nozzle to cause the air to become turbulent and mix with the fuel droplets. The turbulator, also known as a swirl-plate, is an integral part of the entire system and its location has a major influence on the combustion process. It is a circular plate that has sections cut away to cause the air to swirl and increase velocity as shown in Figure 4-1.
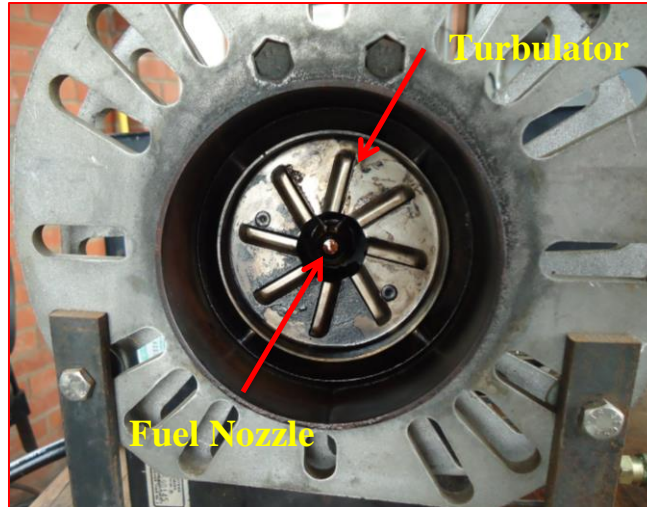
Figure 4-1: Fuel nozzle and turbulator of the stock oil burner.

The turbulator is also adjustable; it can be moved axially along the nozzle axis. A scale from 0 to 5 on the burner is a reference to the turbulator's position with 0 being the closest position to the nozzle and 5 being the furthest away. The standard ignition system for oil burners utilizes a two-electrode system to provide a high voltage spark (plasma) to ignite the mixture of fuel and air. Upon ignition, a light detector signals that a flame has been established, and the high voltage is disconnected to allow the system to operate with a self-sustaining flame.

The burner used for baseline testing is a Riello 40 Series F10 burner (here referred to as the stock burner). Riello is a well-known manufacturer in the industry, and the F10 model is an established oil burner that operates under the previous parameters. It is shown in Figure 4-2 without its cover.
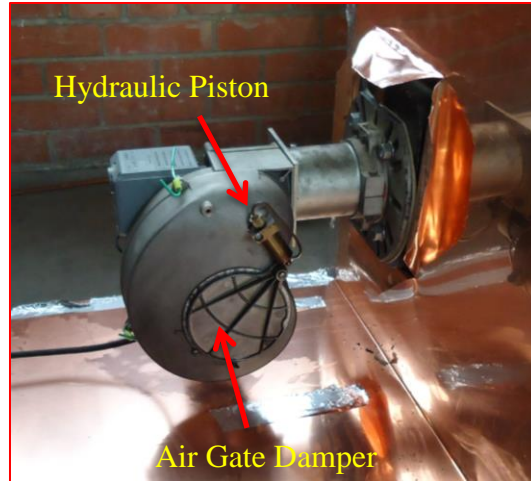
Figure 4-2: Stock burner without cover inserted into boiler.

The modified burner, which is used with the plasma generator, is also a Riello F10 burner that has been modified by Clean Diesel to house the additional hardware required for the plasma formation. Its modifications include a longer burner tube for the electrode wires, a modified turbulator of the same type, and a new control box for the electronics. The light detector is presently not utilized in the modified burner because the plasma is to remain active for the entire combustion duration. The use of similar burners provides a test and control system for comparative results. The differences in the two burners can be seen in Figure 4-3.

Figure 4-3: Stock burner (left) and modified burner (right).

4.1.2 Performance Standards

The performance of oil burners is based not only on the burner itself, but also by the furnace that houses it. The furnace for an oil burner can be described as a combustion chamber that acts as a heat exchanger between the combusting gases and another medium such as water. The size of the furnace determines the surface area for this heat transfer to take place. The standard performance characteristic for burners and furnaces is the Annual Fuel Utilization Efficiency. This considers year-long efficiencies of the system that include non-steady state operation and transient conditions. This factor is not helpful in establishing baseline data for comparisons, which is why the stock burner was also tested. The efficiency of the stock burner can be measured in a state of our own choosing which is convenient for direct comparison. Emission standards are more universal and provide strict limits to use as a reference. Table 4-1

shows emission limits for oil burners that correspond to 90 and 40 ppm for NOx and CO respectively [38,39].

Table 4-1: Oil burner emission limits [38].

Pollutant	Emission Rate In lbs/MMBTU
PM Total	0.012
PM Condensable	0.0094
PM Filterable	0.0030
CO	0.036
TOC / VOC (non methane)	0.0051
NOx	0.13
SOx 0.05%	0.05
SOx 0.25%	0.26

Reference: *Oil Burner Emissions: AP-42 Sept 98 (Jan 2004)*

Riello provided data sheets for their burners that were used as the main reference for emission results, although regional aspects had to be considered. Riello's testing takes place in Massachusetts, which has different conditions than Fort Collins. Altitude is a major factor that could skew results, as well as humidity and air temperature, which is uncontrollable for our testing system. However, Riello's data provides approximate values that give a general idea for results to expect for efficiencies and emission levels. Riello's testing data at Field Settings is shown in Table 4-2. Additional data provided by Riello is shown in Appendix II.

Table 4-2: Riello testing standards at field settings.

Nozzle	Pump Pressure (psi)	Fuel Flow (GPH)	Air Setting	CO2 (%)	O2 (%)	CO (ppm)	Nox (ppm)
1.5, 60B	196	1.98	3.9	12.4	4.04	17	70

These are the target emission values to achieve with the baseline testing of the stock burner, and the goal is to improve these results with the modified burner.

4.2 Burner Testing System

A burner testing system was necessary to act as a medium through which measurements could be made. The system was constructed to resemble a water heating system for the purpose of studying the burners in real-life conditions as opposed to ideal laboratory conditions.

4.2.1 System Design

The burner testing system was constructed at Colorado State University's Engines and Energy Conversion Laboratory where it would have access to the outdoor environment for heat dissipation and an adequate flue gas exhaust. The core components of the system include a furnace to house the burners, a water supply, a water pump, and a heat exchanger. The system was constructed with the intention of measuring thermal efficiency by using a closed water loop. Two 208 liter (55-Gallon) steel drums were filled with water, which were connected with steel fittings to a pump, which then connected to the furnace and the heat exchanger with 3.8 cm (1.5") copper tubing. Water is circulated through the system at flow rates up to 98.5 liters per minute (LPM) by the circulating pump (Taco 2400-50). The heat exchanger (2 Valutech HTL22X25 Radiators) is used as the system load to dissipate the heat that is generated by the burner. This heat sinking scheme allowed this closed system to operate at steady-state conditions within the temperature limits of the furnace and equipment. Its capabilities are enhanced by

61

turning on a 61 cm fan capable of providing 204,000 LPM of forced air through the heat exchanger. The fan is connected to the heat exchanger with a sheet metal hood to ensure that all of the air passes through the heat exchanger. The air then flows through an open window to exit the building. The furnace used for testing is a Pensotti S1-50 and is rated to operate at temperatures above 70 ℃ to prevent condensation of the combustion gases and therefore preventing corrosion on the inside of its cast iron body [40]. For testing purposes, the water should remain below its boiling point (95° C at 0.85 atm) to keep the testing medium in its liquid form, which leaves a small operating temperature window for testing (70 - 95° C). A paddlewheel flow meter (Omega FP7002A/FP7010GI) was installed to measure the volumetric flow of water in the loop, and thermocouples were installed at the furnace inlet and at the furnace outlet. The furnace is essentially a heat exchanger as well; it transfers the heat from the combustion process to the water flowing through it. It consists of seven looped sections that allow the water to circulate around the combustion chamber. The combustion gases then exit the furnace through exhaust duct and outside of the building.

Ambient air conditions were taken into account with a thermocouple and a relative humidity sensor (Dwyer RHU-D). As for the burner, fuel and air flow were measured for AFR calculations, along with the fuel temperature. Fuel flow data was collected by measuring the mass of fuel consumed over a time period with a scale (Adams Equipment 15kg) and stopwatch, and air flow was measured with an anemometer (Sper Scientific 840003) in an air sleeve connected to the air gate of the burner. Off-Road Diesel, also known as red-dyed diesel or #2 diesel, was used for all testing. The fuel was stored in a modified 19 liter tank with a 0.95 cm ID (Inside Diameter) fuel line running through an oil filter and into the burner. The fuel flow rate was controlled by the fuel pressure setting and by the nozzle used. All data except the fuel and

air flow rates was collected by a National Instruments LabVIEW program that logged the data at one-second intervals. The program uses National Instruments Field Point devices (FP-2000 and FP-TC-120) to transfer the data to a computer and into the LabVIEW program. The system schematic is shown in Figure 4-4, and a picture is shown in Figure 4-5.
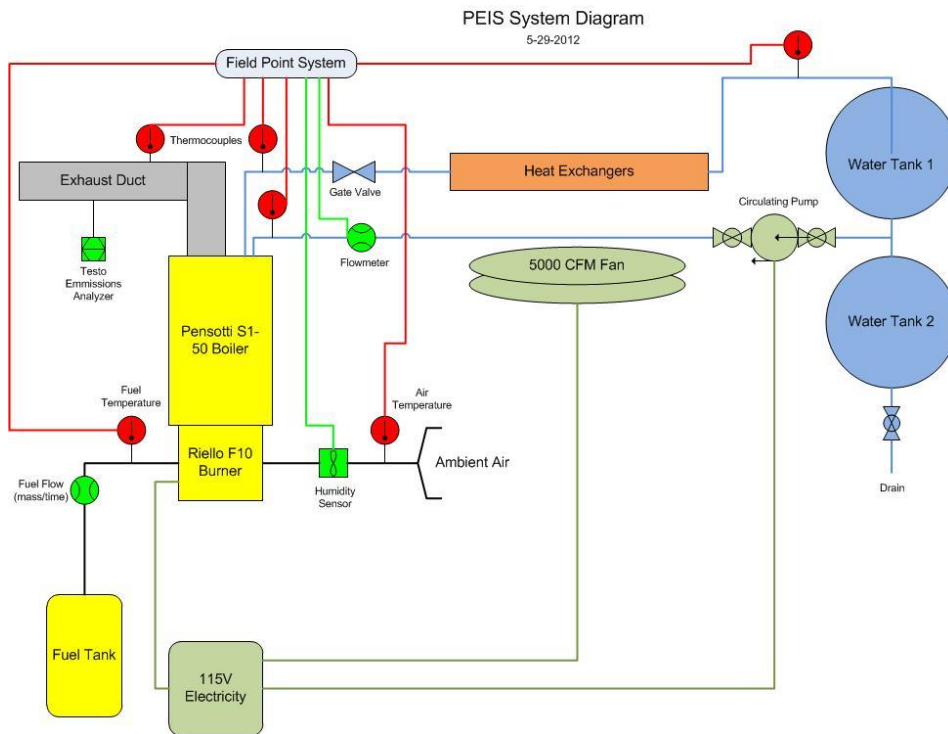
Figure 4-4: Schematic of burner testing system.

Figure 4-5: Burner Testing System: 1) Fuel Filter, 2) Air Sleeve and Anemometer, 3) Fuel Tank, 4) NI FieldPoint System, 5) Heat Exchanger/Fan, 6) Water Pump, 7) Water Tanks, 8) Exhaust Duct.

4.2.2 Thermal Efficiency Calculation

The hardware was designed to measure the thermal efficiency of the system as a whole, as opposed to the burner alone. The heat power added to the circulating water is found as:

$$\dot{Q}_w = \dot{m}_w c_{p,w}(T_2 - T_1) \qquad (4.1)$$

where $\dot{m}_w$ is the mass flow of water, $c_{p,w}$ is the specific heat of water (held constant at 4200 J/kg*K), T_2 is the furnace outlet temperature, T_1 is the furnace inlet temperature, and $\dot{Q}_w$ is the heat transfer rate to the water. On the fuel side, the heating content of fuel per unit mass per time is

considered. Diesel fuel was used for all burner testing because of its similar properties to No. 2 fuel oil which has a heating content of approximately 46,250 kJ/kg (142,000 BTU per gallon) [41]. This number is held constant for all test results. Therefore the input heat transfer rate, $\dot{Q}_f$, is

$$\dot{Q}_f = (4.625 \text{ x } 10^7 \text{ J/kg})*\dot{m}_f \qquad (4.2)$$

where $\dot{m}_f$ is the mass flow of fuel. The thermal efficiency is then found as:

$$\eta_{thermal} = \frac{\dot{Q}_w}{\dot{Q}_f} \qquad (4.3)$$

For this method of calculating thermal efficiency to be accurate for comparative purposes, the testing of the stock and modified burners needed to be performed under very similar conditions.

4.2.3 Emission Measurements

The other aspect of the burner testing is the emission results. For these measurements, a Testo 330-1 Emissions Analyzer was installed into the exhaust duct of the furnace, approximately 60 cm from the furnace outlet. The analyzer measures levels of O_2, CO_2, CO, and NOx, as well as the overall combustion efficiency (calculated by an equation created by Testo [42] as shown in Appendix III; it did not provide helpful information for burner performance) and exhaust temperature. A thermocouple was also installed approximately 15 cm from the furnace outlet for another exhaust temperature measurement. This temperature was typically

higher than that of the emission analyzer's, most likely due to its location closer to the combustion chamber. The data from the analyzer was used with Testo EasyHeat software to log data at one-second intervals. The targeted emission gases that needed to be reduced were CO and NOx, and their values provided a quick evaluation of the effectiveness of the combustion taking place.

4.3   Stock Burner

The stock burner was tested to provide baseline data. The burner was first cleaned and tuned to operate at optimum conditions. A 1.00 GPH nozzle with a 60°, solid spray angle (known as a Type B spray pattern) designed for fuel flow of approximately 3.8 liters per hour (LPH) was used for testing. Diesel fuel was stored in a tank that gravity fed the fuel pump, and the fuel pressure was adjusted to 965 kPa (140 psi) for this particular nozzle. An air duct was retro-fitted onto the air gate of the burner to measure the air flow with the anemometer. Upon connecting the stock burner to power (120 VAC), its motor is activated and turns the fan to purge the combustion chamber for 14 seconds. Prior to ignition, the light detector sees no light, causing a solenoid valve to open to pass fuel to the nozzle. A high voltage is then sent through the ignition electrodes to ignite the fuel-air mixture. The light detector then shuts off the high voltage when it sees that a flame has been established. The burner was inserted into the furnace for testing, and was only operated when water is being pumped through the furnace.

4.3.1   Testing Methodology

To maintain a constant fuel supply for both burners, the same type of fuel, fuel temperature, fuel nozzle, and fuel pressure were required. The oxidizer (air supply) was used as a variable to allow for different AFR's. Through preliminary testing, it was found that the heat exchanger was not able to dissipate the exact amount of heat produced by the burner, meaning the temperature of the water did not remain constant. It was decided that the water should be heated to its optimal operating temperature between 70-95 degrees Celsius before applying the heat exchanger. This allowed the system to bring the temperature up quickly, before slowing down its rate of change to simulate an approximate steady-state condition. Data was analyzed during steady-state operation which typically lasted approximately 10 minutes. An example set of data is shown here in Figure 4-6.
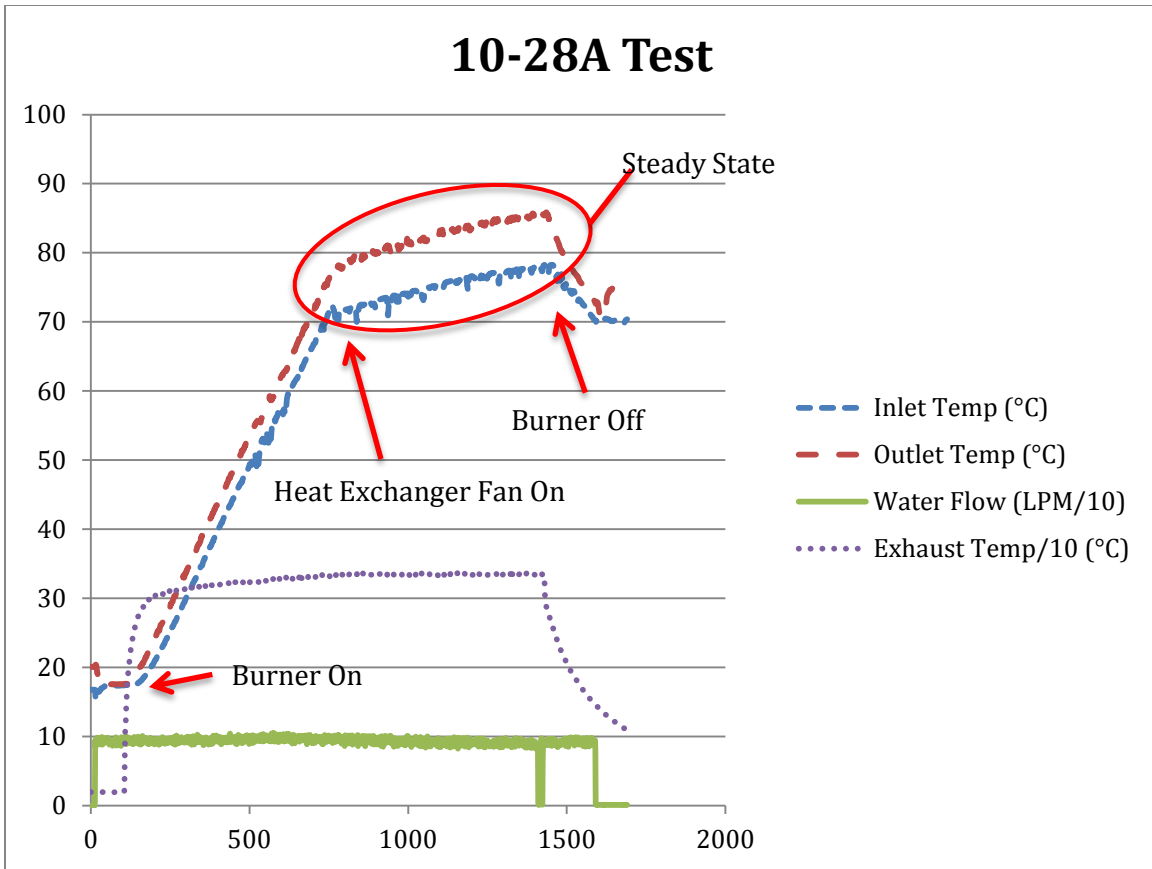
Figure 4-6: Sample plot of testing data.

As for the emissions data, the analyzer collected and logged data through the entire duration of the test to show the results of combustion during startup, steady-state, and shut down conditions. An example of the emissions data during a test is shown in Figure 4-7. Note the spikes in CO during startup and shutdown of the burner due to incomplete combustion.
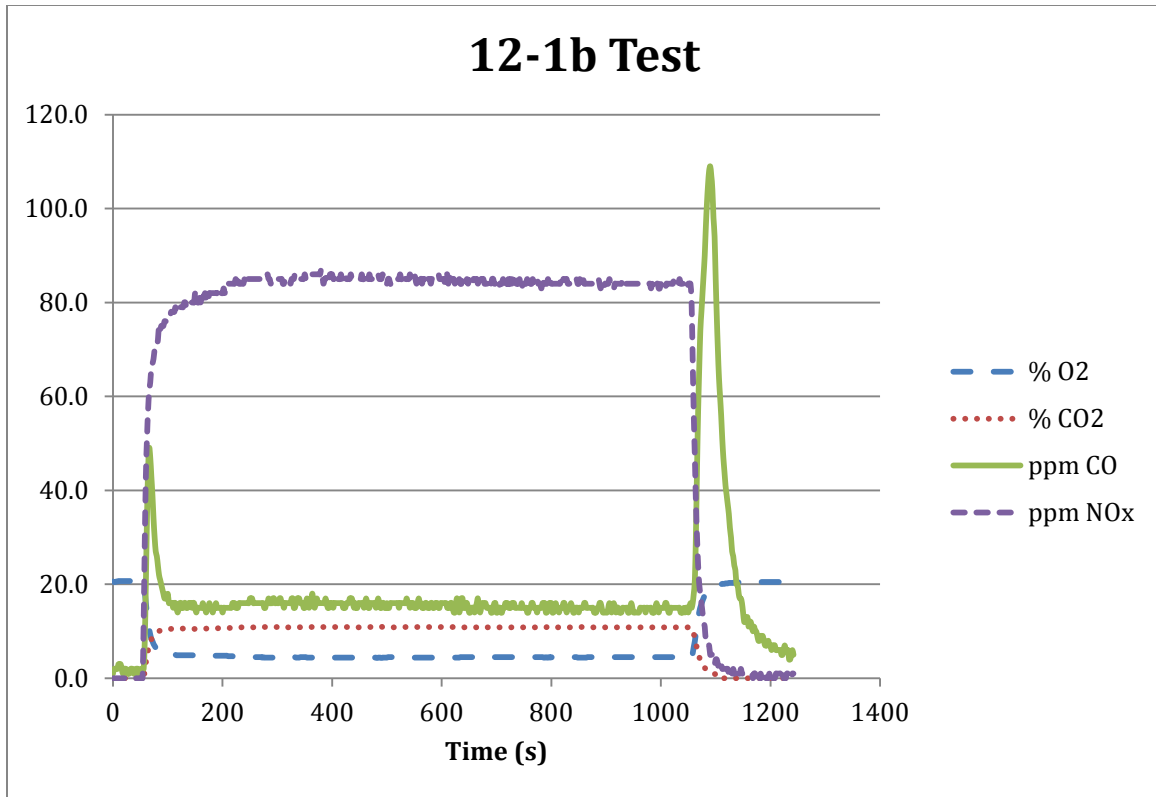
Figure 4-7: Sample plot of emissions data.

The testing methodology consisted of adjusting the stock burner settings to determine its most efficient operating parameters that produced pollutant gases within the emission limits of Table 4-1. This condition was found with adjustments to the turbulator setting and the AFR. The fuel system was to remain constant, so the AFR was adjusted by the air gate. The initial test of the burner started with air and turbulator settings at or near Riello's recommendations according to the corresponding fuel settings (pressure and nozzle size). Data was collected for this setting, and the emission's data was analyzed. The amount of carbon monoxide in the exhaust was used as the main indication of the combustion process. Riello's data showed CO levels as low as 17 ppm (Table 4-2) under their testing conditions, and that value was used as a target. Upon completing a test with a given air and turbulator setting, the settings were then adjusted to

attempt to improve its performance. Through multiple preliminary tests it was discovered that, in general, high levels of CO signaled the need for more air. Adjustments were systematically made to provide results of a range of settings based on reasonable emission levels and Riello's specifications.

4.3.2   Stock Burner Results

The stock burner testing results used for comparisons to the modified burner utilized a 1.00 GPH, 60° solid spray nozzle at a fuel pressure of 956 kPa (140 psi). Table 4-3 shows the results of 10 settings and Table 4-4 shows the best test results from Table 4-3. The most important data, such as thermal efficiency, CO and NOx emissions, are highlighted.

Table 4-3: Stock burner testing data performed on 12-10-11.

Stock Burner Testing Data (12-10)

		12-10a	12-10b	12-10c	12-10f	12-10e	12-10d	12-10g	12-10k	12-10j	12-10i
	Test Name	12-10a	12-10b	12-10c	12-10f	12-10e	12-10d	12-10g	12-10k	12-10j	12-10i
	Date/Time	12-10, 11:50 AM	12-10, 12:05 PM	12-10, 12:25 PM	12-10, 1:15 PM	12-10, 1:00 PM	12-10, 12:40 PM	12-10, 1:30 PM	12-10, 2:30 PM	12-10, 2:15 PM	12-10, 2:00 PM
	Sampling Period	11:52:08 - 11:59:38	12:08:27 - 12:16:22	12:26:01 - 12:34:21	1:18:16 - 1:26:36	1:01:07 - 1:10:17	12:44:02 - 12:52:22	1:34:31 - 1:42:51	2:34:08 - 2:42:28	2:17:49 - 2:26:59	2:01:46 - 2:10:06
Settings	Nozzle Size	1	1	1	1	1	1	1	1	1	1
	Pump Pressure	140	140	140	140	140	140	140	140	140	140
	Turbulator Setting	1	1	1	1.5	1.5	1.5	1.5	2	2	2
	Air Setting	2	2.4	2.8	2	2.4	2.8	3.2	2	2.4	2.8
Fuel	Avg Fuel Temp	14.64	15.16	15.59	17.69	16.17	15.15	18.53	22.81	21.65	21.90
	StDev	0.23	0.34	0.21	0.49	0.15	0.14	0.28	0.36	0.34	0.22
	Initial Fuel Mass (kg)	9.17	9.17	9.17	11.54	12.29	13.28	10.75	7.98	8.7	9.84
	Final Fuel Mass (kg)	8.540	8.54	8.54	10.82	11.59	12.48	10.1	7.33	8.03	8.92
	Time Measured (min)	9.892	9.892	9.892	11.309	10.971	12.624	10.281	10.254	10.478	14.486
	Fuel Flow Rate (kg/min)	0.0637	0.0637	0.0637	0.0637	0.0638	0.0634	0.0632	0.0634	0.0639	0.0635
	Actual GPH	1.1794	1.1794	1.1794	1.1790	1.1816	1.1735	1.1708	1.1739	1.1841	1.1761
Air	Avg Humidity (%)	30.17	31.18	31.11	29.63	30.12	31.11	29.00	27.99	28.35	27.87
	StDev	1.20	1.74	1.61	1.54	1.60	1.69	1.40	1.46	1.43	1.28
	Avg Ambient Temp	14.49	14.72	14.86	15.59	15.66	15.03	16.16	17.52	17.43	18.28
	StDev	0.16	0.34	0.12	0.44	0.21	0.36	0.20	0.22	0.36	0.76
	Air Velocity (ft/min)	1003	1115	0	1021	1166	1272	1399	1035	1183	1280
	Air Flow Rate (kg/min)	1.046	1.162	0.000	1.064	1.215	1.326	1.458	1.079	1.233	1.334
	Air-Fuel Ratio	16.417	18.250	0.000	16.717	19.050	20.924	23.066	17.020	19.285	21.009
Heat Transfer	Avg Flow Rate (GPM)	25.97	25.81	25.96	25.96	26.00	25.95	26.00	25.98	25.97	25.99
	StDev Flow Rate (GPM)	0.79	0.76	0.80	0.75	0.80	0.80	0.74	0.82	0.77	0.77
	Avg dT	5.49	5.62	5.58	5.53	5.53	5.50	5.29	5.36	5.37	5.40
	StDev dT	0.18	0.18	0.18	0.18	0.18	0.18	0.18	0.17	0.17	0.16
	Q (J/min)	2268397	2309977	2304501	2287158	2290468	2273223	2187808	2218761	2221090	2232157
	Q Error (+/-)	100246	98245	96018	99891	103996	106369	97707	99354	101222	94281
	BTU/hour	129002	131366	131055	130068	130257	129276	124419	126179	126311	126941
	BTU/hour Error (+/-)	5701	5587	5460	5681	5914	6049	5556	5650	5756	5362
Emissions	O2 (%)	2.79	4.41	6.20	2.84	5.09	6.58	7.66	3.24	5.38	6.85
	StDev	0.03	0.03	0.00	0.06	0.02	0.05	0.05	0.05	0.05	0.05
	CO2 (%)	13.62	12.41	11.06	13.58	11.89	10.78	9.97	13.28	11.68	10.58
	StDev	0.02	0.02	0.00	0.02	0.02	0.04	0.04	0.04	0.04	0.04
	CO (ppm)	306.40	41.95	62.26	289.40	50.29	57.80	109.12	249.12	59.93	65.09
	StDev	38.69	3.26	2.76	40.27	3.72	3.22	2.05	28.87	4.72	2.44
	NOx (ppm)	75.55	77.99	69.92	69.88	70.50	67.48	65.04	66.83	67.26	65.09
	StDev	0.64	0.79	0.67	0.54	0.82	0.63	0.45	0.72	0.71	0.52
	Exhaust Temp (TC)	227.65	240.64	250.86	234.01	245.58	254.26	260.45	236.06	248.32	258.89
	StDev	0.51	0.67	0.83	0.81	0.82	0.78	0.75	0.60	0.82	1.36
	Exhaust Temp Testo	205.37	217.85	228.59	211.64	223.18	231.80	236.89	213.80	225.18	235.41
	StDev	1.75	1.43	0.96	1.95	1.17	0.90	2.00	1.83	1.54	0.24
	% Excess Air	14.24	24.85	39.20	14.52	29.96	42.73	53.78	17.05	32.20	45.39
	StDev	0.20	0.20	0.00	0.35	0.17	0.50	0.53	0.30	0.41	0.45
Performance	Combustion Efficiency	86.82	85.75	84.34	86.65	85.26	83.99	83.01	86.54	85.14	83.75
	StDev	0.06	0.06	0.06	0.07	0.06	0.05	0.11	0.06	0.06	0.05
	Input BTU	165117	165117	165117	165060	165419	164296	163913	164344	165779	164655
	Output BTU	129002	131366	131055	130068	130257	129276	124419	126179	126311	126941
	Output BTU StDev	5701	5587	5460	5681	5914	6049	5556	5650	5756	5362
	Thermal Efficiency	78.13%	79.56%	79.37%	78.80%	78.74%	78.68%	75.91%	76.78%	76.19%	77.10%
	Thermal Efficiency Error	3.45%	3.38%	3.31%	3.44%	3.58%	3.68%	3.39%	3.44%	3.47%	3.26%

Table 4-4: Best stock burner testing results performed on 12-10-11.

Stock Burner Testing Data (12-10)

	Test Name	12-10b	12-10c	12-10e	12-10d	12-10j
	Date/Time	12-10, 12:05 PM	12-10, 12:25 PM	12-10, 1:00 PM	12-10, 12:40 PM	12-10, 2:15 PM
	Sampling Period	12:08:27 - 12:16:22	12:26:01 - 12:34:21	1:01:07 - 1:10:17	12:44:02 - 12:52:22	2:17:49 - 2:26:59

Settings	Nozzle Size	1	1	1	1	1
	Pump Pressure	140	140	140	140	140
	Turbulator Setting	1	1	1.5	1.5	2
	Air Setting	2.4	2.8	2.4	2.8	2.4

Fuel	Avg Fuel Temp	15.16	15.59	16.17	15.15	21.65
	StDev	0.34	0.21	0.15	0.14	0.34
	Initial Fuel Mass (kg)	9.17	9.17	12.29	13.28	8.7
	Final Fuel Mass (kg)	8.54	8.54	11.59	12.48	8.03
	Time Measured (min)	9.892	9.892	10.971	12.624	10.478
	Fuel Flow Rate (kg/min)	0.0637	0.0637	0.0638	0.0634	0.0639
	Actual GPH	1.1794	1.1794	1.1816	1.1735	1.1841

Air	Avg Humidity (%)	31.18	31.11	30.12	31.11	28.35
	StDev	1.74	1.61	1.60	1.69	1.43
	Avg Ambient Temp	14.72	14.86	15.66	15.03	17.43
	StDev	0.34	0.12	0.21	0.36	0.36
	Air Velocity (ft/min)	1115 x		1166	1272	1183
	Air Flow Rate (kg/min)	1.162 x		1.215	1.326	1.233
	Air-Fuel Ratio	18.250 x		19.050	20.924	19.285

Heat Transfer	Avg Flow Rate (GPM)	25.81	25.96	26.00	25.95	25.97
	StDev Flow Rate (GPM)	0.76	0.80	0.80	0.80	0.77
	Avg dT	5.62	5.58	5.53	5.50	5.37
	StDev dT	0.17	0.16	0.18	0.19	0.19
	Q (J/min)	2309977	2304501	2290468	2273223	2221090
	Q Error (+/-)	98245	96018	103996	106369	101222
	BTU/hour	131366	131055	130257	129276	126311
	BTU/hour Error (+/-)	5587	5460	5914	6049	5756

Emissions	O2 (%)	4.41	6.20	5.09	6.58	5.38
	StDev	0.03	0.00	0.02	0.05	0.05
	CO2 (%)	12.41	11.06	11.89	10.78	11.68
	StDev	0.02	0.00	0.02	0.04	0.04
	CO (ppm)	41.95	62.26	50.29	57.80	59.93
	StDev	3.26	2.76	3.72	3.22	4.72
	NOx (ppm)	77.99	69.92	70.50	67.48	67.26
	StDev	0.79	0.67	0.82	0.63	0.71
	Exhaust Temp (TC)	240.64	250.86	245.58	254.26	248.32
	StDev	0.67	0.83	0.82	0.78	0.82
	Exhaust Temp Testo	217.85	228.59	223.18	231.80	225.18
	StDev	1.43	0.96	1.17	0.90	1.54
	% Excess Air	24.85	39.20	29.96	42.73	32.20
	StDev	0.20	0.00	0.17	0.50	0.41

Performance	Combustion Efficiency	85.75	84.34	85.26	83.99	85.14
	StDev	0.06	0.06	0.06	0.05	0.06
	Input BTU	165117	165117	165419	164296	165779
	Output BTU	131366	131055	130257	129276	126311
	Output BTU StDev	5587	5460	5914	6049	5756
	Thermal Efficiency	79.56%	79.37%	78.74%	78.68%	76.19%
	Thermal Efficiency Error	3.38%	3.31%	3.58%	3.68%	3.47%

Note that Riello's CO emissions were not achieved during these tests, most likely due to the use of a 1.00 GPH nozzle instead of the 1.5 GPH nozzle used in Riello's tests. Earlier testing with a 1.5 GPH nozzle did achieve CO emissions near 17 ppm, although NOx exceeded Riello's standards by approximately 10 ppm as shown in Appendix IV.

4.4   Modified Burner

As mentioned previously, the modified burner is also a Riello F10 model that has been retrofitted for use of the plasma generator. Six strands of welding wire were permanently installed into the body of the burner, where they can be connected to the plasma generator's electrode bolts. The wires go through the burner tube and are connected to three Riello electrode assemblies (each assembly has two electrodes) as shown in Figure 4-8.

Figure 4-8: Modified burner - A) Electrodes and turbulator, B) Connection to plasma generator.

The electrode tips are insulated with ceramic tubing to prevent arcing to the turbulator and nozzle. The turbulator was trimmed away in places for all of the electrodes to fit around the nozzle, and insulated in a dielectric material to prevent arcing. The electrode tips were centered around the nozzle with an electrode distance of 10-11 mm. With the proper set up of the electrodes, a stable plasma was formed in open air conditions as shown in Figure 4-8-A.

The electronic system for the modified burner was different than that of the stock burner, as the ignition system was controlled with the plasma generator. Two switches on the burner control box were used to turn on the burner's motor and to open the solenoid valve for the fuel. This valve required an external power supply due to the removal of its electronics in the control box. A Variac generator was used to provide 4 Volts to the valve's coils. Operation of the modified burner started with the formation of the plasma with the plasma generator. Once the plasma was formed (confirmed audibly when installed in boiler), the burner motor was turned on, and then the solenoid valve was opened to pump fuel through the nozzle. Under suitable AFR conditions, the fuel-air mixture was ignited by the plasma. The interaction of the mixture with the plasma can be seen in Figure 4-9 (the burner tube and turbulator were removed for access).

Figure 4-9: Combustion of fuel without the use of the turbulator or burner tube in the modified burner.

4.4.1 Modified Burner Testing

The modified burner was tested in the same manner as the stock burner, although it was more difficult to set up. Initial attempts to use the modified burner with the testing system were plagued by electromagnetic interference (EMI) caused by the plasma generator. The affected devices included the water flow meter, fuel scale, and the emissions analyzer. The remedy for this interference was shielding of the burner and plasma generator with a box made from copper sheet metal, and shielding of all equipment wiring with aluminum foil. For a test, the water pump was first turned on to allow water to flow through the system. The plasma generator was then turned on, followed by the air supply, and then the fuel supply. Ignition could be heard inside the furnace and verified by the rapid increase of exhaust temperature.

Unlike the stock burner, the turbulator in the modified burner was fixed. Its location was determined by finding a place where minimal arcing occurred between it and the plasma. The only control of the combustion process was therefore the air setting, which operated in the same manner as the stock burner. Since Riello's specifications for the air setting were not applicable for this burner, the ideal air setting was found experimentally by examining emission results.

Two methods were used for the modified burner testing: plasma ignition and plasma combustion. Plasma ignition mode worked like the stock burner; the plasma was used to ignite the flame and was then shut off. The collected data then showed the results of a self-sustaining flame. On the other hand, plasma combustion mode used the plasma for the entire duration of the test. Comparing these two modes provided an even better (more direct) assessment of the plasma effects.

4.4.2 Modified Burner Results

Table 4-5: Results of the modified burner in plasma combustion mode.

Plasma Burner Testing Data (At 12-15 Setting)

		12-15PBg	12-15PBh	12-15PBi	12-15PBe	12-15PBf
	Test Name	12-15PBg	12-15PBh	12-15PBi	12-15PBe	12-15PBf
	Date/Time	12-15, 3:15 PM	12-15, 3:30 PM	12-15, 3:50 PM	12-15, 2:25 PM	12-15, 3:00 PM
	Sampling Period	3:18:07 - 3:25:12	3:31:42 - 3:40:02	3:50:19 - 3:58:14	2:28:17 - 2:35:47	3:02:46 - 3:09:51
Settings	Nozzle Size	1	1	1	1	1
	Pump Pressure	140	140	140	140	140
	Turbulator Setting	x	x	x	x	x
	Air Setting	1.9	2	2.3	2.5	2.8
Fuel	Avg Fuel Temp	22.49	23.28	24.33	21.55	21.64
	StDev	0.10	0.11	0.10	0.06	0.07
	Initial Fuel Mass (kg)	11.05	10.42	9.74	7.86	11.67
	Final Fuel Mass (kg)	10.470	9.78	9.11	7.29	11.09
	Time Measured (min)	9.252	10.143	10.003	9.083	9.166
	Fuel Flow Rate (kg/min)	0.0627	0.0631	0.0630	0.0628	0.0633
	Actual GPH	1.1609	1.1685	1.1663	1.1621	1.1718
Air	Avg Humidity (%)	23.09	23.27	24.11	23.58	22.83
	StDev	1.53	1.49	1.68	1.61	1.45
	Avg Ambient Temp	25.14	25.71	25.58	25.00	25.41
	StDev	0.33	0.15	0.12	0.41	0.20
	Air Velocity (ft/min)	x	x	x	x	x
	Air Flow Rate (kg/min)	x	x	x	x	x
	Air-Fuel Ratio	x	x	x	x	x
Heat Transfer	Avg Flow Rate (GPM)	25.82	25.82	25.92	25.86	25.83
	StDev Flow Rate (GPM)	0.82	0.78	0.75	0.78	0.81
	Avg dT	5.32	5.20	5.18	5.15	5.08
	StDev dT	0.18	0.23	0.16	0.20	0.30
	Q (J/min)	2186407	2137724	2135669	2121685	2087112
	Q Error (+/-)	102030	115969	91316	103794	140158
	BTU/hour	124339	121570	121453	120658	118692
	BTU/hour Error (+/-)	5802	6595	5193	5903	7971
Emissions	O2 (%)	3.31	3.96	5.60	6.65	7.62
	StDev	0.03	0.06	0.05	0.07	0.04
	CO2 (%)	13.23	12.74	11.51	10.73	10.00
	StDev	0.02	0.04	0.04	0.05	0.03
	CO (ppm)	21.79	12.16	9.45	6.54	15.00
	StDev	2.06	1.01	0.80	0.72	1.13
	NOx (ppm)	112.10	113.28	104.23	94.60	78.22
	StDev	0.55	0.53	0.57	1.16	0.63
	Exhaust Temp (TC)	239.95	243.16	252.48	257.33	262.94
	StDev	1.26	2.05	1.49	0.77	1.18
	Exhaust Temp Testo	219.06	221.51	229.82	235.23	240.77
	StDev	2.63	4.04	3.52	2.50	2.90
	% Excess Air	17.54	21.74	34.09	43.43	53.31
	StDev	0.15	0.36	0.39	0.67	0.44
Performance	Combustion Efficiency	86.61	86.25	85.11	84.19	83.29
	StDev	0.10	0.14	0.13	0.08	0.12
	Input BTU	162527.42	163586.64	163284.35	162697.10	164052.34
	Output BTU	124339	121570	121453	120658	118692
	Output BTU StDev	5802	6595	5193	5903	7971
	Thermal Efficiency	76.50%	74.32%	74.38%	74.16%	72.35%
	Thermal Efficiency Error	3.57%	4.03%	3.18%	3.63%	4.86%

Table 4-5 shows the results of the modified burner acting in plasma combustion mode. It is clearly seen that the CO levels are much lower than that of the stock burner tests. Note that an air setting of 1.7 was tested, but produced extreme CO emissions (1000+ ppm). This test is not shown in Table 4-5. Generally, when emissions showed extremely high values of CO or NOx, the data was not analyzed and that setting was rejected. To see the difference between plasma combustion mode and plasma ignition mode, another test was performed with the settings of the best combustion mode test. The results of this comparison are shown in Table 4-6 and include the results of a similar stock burner test.

Table 4-6: Summary of burner testing.

Plasma Burner Testing Data (At 12-15 Setting)

Test Name	12-15PBi	12-15PBJ	12-15L
Date/Time	12-15, 3:50 PM	12-15, 4:05 PM	12-15, 5:30 PM
Sampling Period	3:50:19 - 3:58:14	4:06:57 - 4:16:57	5:33:31 - 5:42:41

12-15PBi (Left): Plasma Combustion
12-15PBJ (Middle): Plasma Ignition Only
12-15L (Right): Stock Burner

		12-15PBi	12-15PBJ	12-15L
Settings	Nozzle Size	1	1	1
	Pump Pressure	140	140	140
	Turbulator Setting	x	x	1
	Air Setting	2.3	2.3	2.4
Fuel	Avg Fuel Temp	24.33	25.11	17.18
	StDev	0.10	0.08	0.27
	Initial Fuel Mass (kg)	9.74	8.89	10.51
	Final Fuel Mass (kg)	9.11	8.24	9.87
	Time Measured (min)	10.003	10.425	10.381
	Fuel Flow Rate (kg/min)	0.0630	0.0624	0.0617
	Actual GPH	1.1663	1.1546	1.1417
Air	Avg Humidity (%)	24.11	23.27	28.38
	StDev	1.68	1.47	1.30
	Avg Ambient Temp	25.58	26.39	22.18
	StDev	0.12	0.33	0.75
	Air Velocity (ft/min)	x	x	x
	Air Flow Rate (kg/min)	x	x	x
	Air-Fuel Ratio	x	x	x
Heat Transfer	Avg Flow Rate (GPM)	25.92	25.84	25.92
	StDev Flow Rate (GPM)	0.75	0.76	0.79
	Avg dT	5.18	5.32	5.44
	StDev dT	0.16	0.20	0.18
	dQ (J/min)	2135669	2189129	2242410
	dQ Error (+/-)	91316	104123	100590
	BTU/hour	121453	124494	127524
	BTU/hour Error (+/-)	5193	5921	5720
Emissions	O2 (%)	5.60	5.43	4.50
	StDev	0.05	0.05	0.06
	CO2 (%)	11.51	11.64	12.34
	StDev	0.04	0.03	0.04
	CO (ppm)	9.45	8.42	33.26
	StDev	0.80	1.10	2.19
	NOx (ppm)	104.23	97.91	80.55
	StDev	0.57	0.69	0.82
	Exhaust Temp (TC)	252.48	252.81	242.96
	StDev	1.49	0.66	1.06
	Exhaust Temp Testo	229.82	231.65	222.80
	StDev	3.52	1.98	2.47
	% Excess Air	34.09	32.65	25.48
	StDev	0.39	0.40	0.42
Performance	Combustion Efficiency	85.11	85.13	85.80
	StDev	0.13	0.06	0.10
	Input BTU	163284.35	161648.46	159836.17
	Output BTU	121453	124494	127524
	Output BTU StDev	5193	5921	5720
	Thermal Efficiency	74.38%	77.02%	79.78%
	Thermal Efficiency Error	3.18%	3.66%	3.58%

The results of the burner testing can be summarized by Figure 4-10, which shows the best results of the stock burner and modified burner acting in plasma ignition and combustion mode.
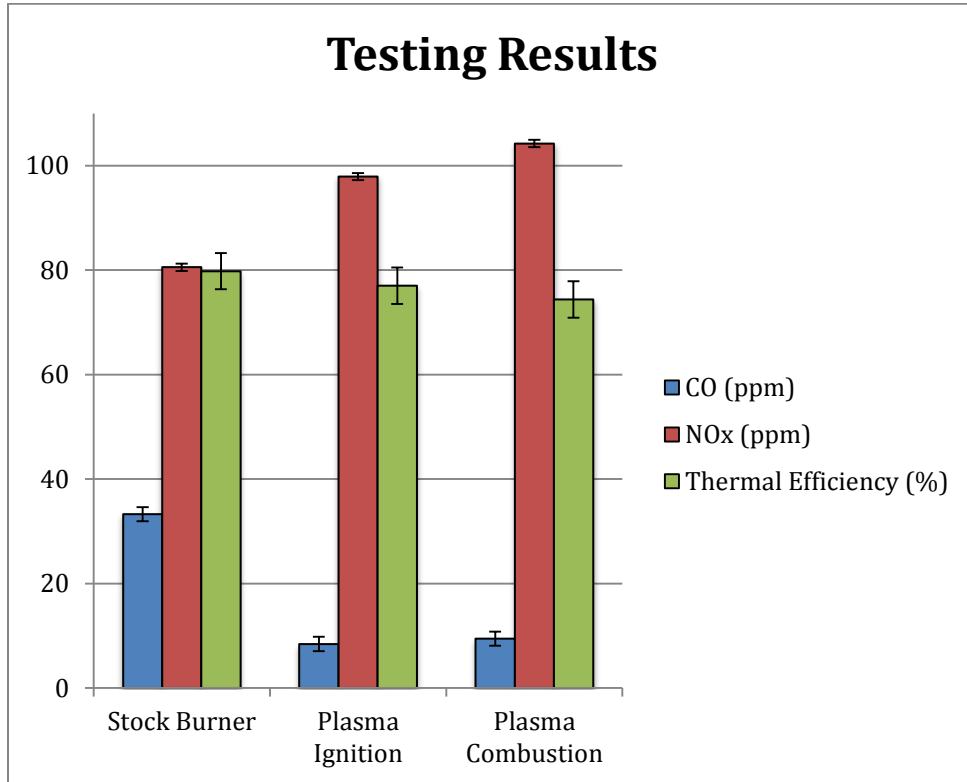
Figure 4-10: Testing results of stock and modified burner.

4.4.3   Discussion of Testing Results

Comparison of the results between the stock burner and the modified burner in plasma ignition and plasma combustion modes suggest that the application of the plasma generator shows no significant benefits. Figure 4-10 shows that CO emissions are reduced in the modified burner, while NOx is higher than with the stock burner. This is most likely due to the hardware modifications though, not the application of plasma. Significant differences would be seen

between plasma ignition and plasma combustion mode if this were the case. As for the thermal efficiency, the use of plasma seems to have no benefit. These results show that the use of the plasma surely does not aid the system enough to compensate for its electrical power consumption.

To investigate the reasons for this, the plasma formation on the burner was examined closely. Under no-flow conditions, a solid and uniform plasma is created. However, the addition of air flow to the plasma causes it to create a ring shape along the electrode tips. The differences in the flow conditions are shown in Figure 4-11. These pictures confirm what was seen in the ICCD images from Chapter 2: the addition of air flow separates the plasma into shorter paths, thus reducing the volume of the plasma.
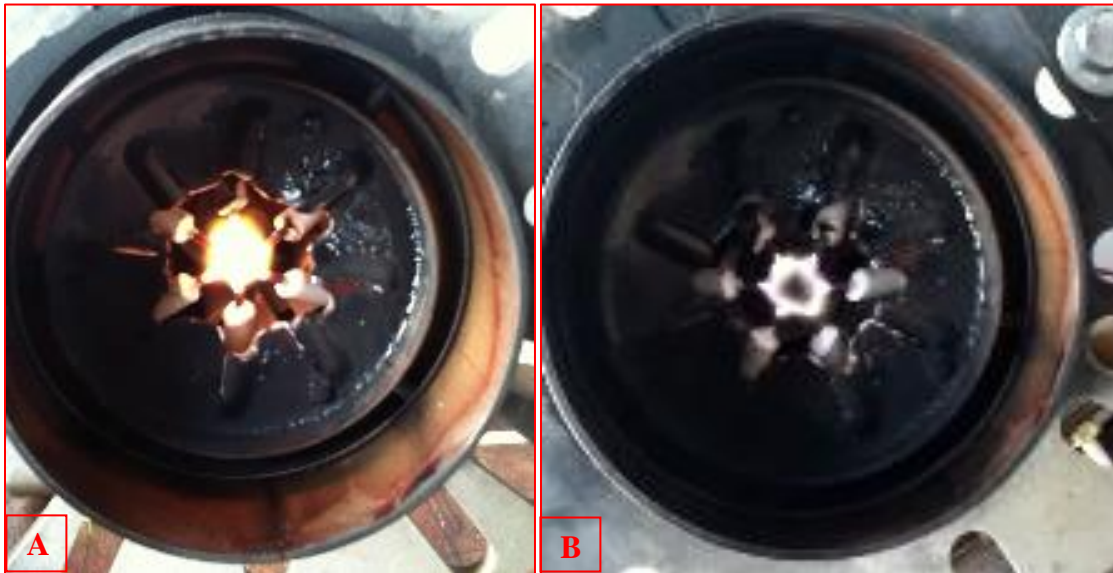
Figure 4-11: A) Plasma formation with no air flow, B) Plasma formation with air flow.

With this visual analysis and the evidence of the ineffectiveness through testing, it appears likely that the plasma is not interacting with the fuel enough to significantly reform it. The nozzle used

in these tests was of the solid spray type, which suggests the majority of the fuel is passing straight through the non-ionized region of the "plasma ring" that is caused by the air and fuel flow. Additionally, it is possible that the transit time of the air-fuel mixture with the plasma is less than that needed for chemical reactions to occur. To improve the fuel reforming capabilities of the plasma, it may be useful to increase the transit time of fuel molecules by reducing the flow speed.

4.5   Additional Testing

With the realization that the plasma needs to interact more thoroughly with the fuel-air mixture, additional tests were performed to improve the fuel reforming capabilities. Initially, it was postulated that the "plasma ring" formation could be eliminated by reducing the air flow through the plasma. A conceptual design was developed to restrict the amount of air flow that travels through the plasma region and instead allows air to flow around the plasma before it mixes with the fuel. This design is shown in Figure 4-12.
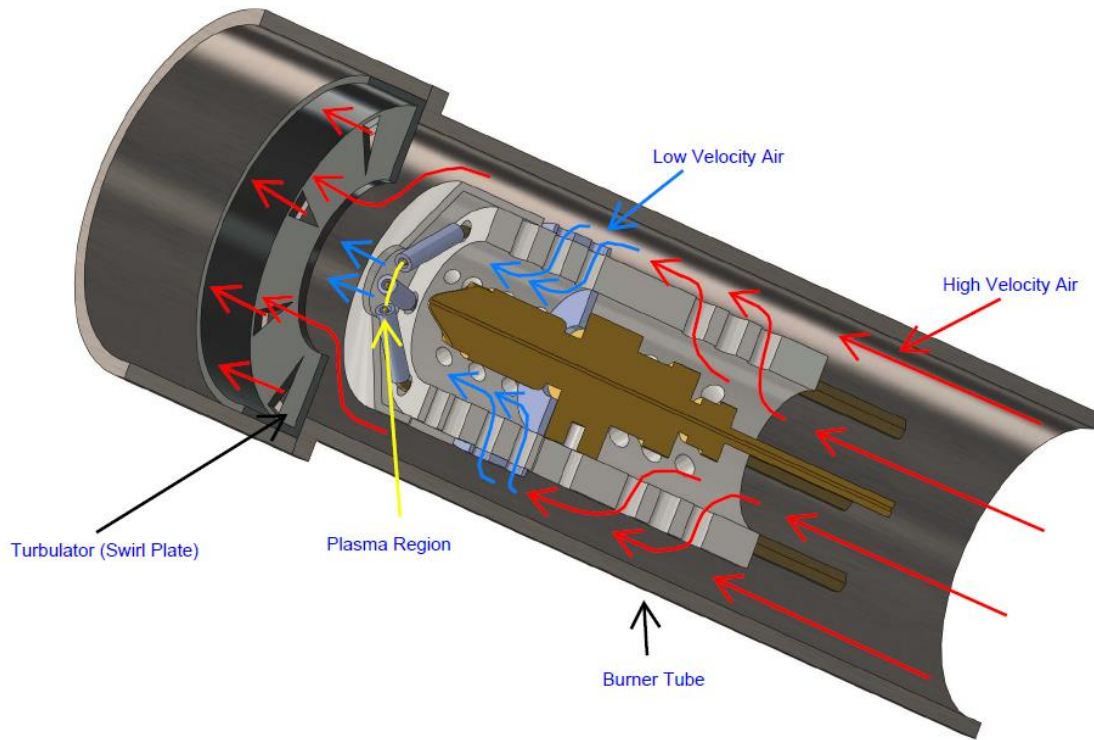
Figure 4-12: SolidWorks cross-section design of proposed plasma-shielding design.

This approach would be similar to the reforming processes discussed in Chapter 1 where the intention is to partially oxidize the fuel as it interacts with the plasma to produce syngas then fully oxidize the hydrogen rich fuel for combustion. The intent was to allow the plasma to interact with the fuel in the largest volumetric shape possible. However, it was soon realized that the fuel flow alone caused the formation of the plasma ring, and the model was abandoned. While this was an unsuccessful attempt to improve the plasma fuel reformer, it pointed out that there is no way to escape the plasma ring with the given equipment since the plasma is so easily perturbed by introducing flow.

4.5.1   Hollow Spray Nozzle

Previous test results came with the use of the 1.00 GPH 60° solid spray nozzle, and visual analysis suggests that most of the fuel misses the plasma region during operation. To counteract this situation, tests were performed with a nozzle designed to spray the fuel in a hollow shape (Type A hollow spray nozzle) that would make the best use of the ring formation of the plasma. Initial open-air tests showed that this setup caused obstruction of the fuel spray with the electrode insulators. To prevent this obstruction, new electrode insulators were made that left the electrode tips exposed. Open air tests showed that this new formation would arc to the turbulator with air flow unless the turbulator was as far away as possible from the electrodes (similar to the 5 setting of the stock burner). The burner was tested in the furnace, but CO levels never reached less than 100 ppm for any air-fuel ratio (AFR), so the approach was not pursued further.

Chapter 5

Conclusions

The plasma generator provided by Clean Diesel LLC was analyzed by its electrical characteristics and through optical emission spectroscopy. It was determined that the peak voltages during the discharge measured between 4-6 kV (with respect to earth ground) and peak current was between 1-2 A. Based on the discharge current of the plasma generator and the diagram of plasma regimes in Figure 1-4, it is assumed that the plasma is operating in the glow-to-arc regime. The use of a floating ground on the secondary transformer windings prevented the finding of the potential difference between electrodes, and thus prevented the measurement of the electric field created by the plasma. The plasma generator frequency, defined as the frequency of a discharge from any electrode, could be adjusted, but variation in the plasma generator frequency showed no noticeable effects in the plasma characterization.

Optical emission spectroscopy was performed on the plasma generator which focused on determining vibrational and rotational temperatures of the second positive system of nitrogen and using Stark broadening of Balmer series lines to find the electron temperature and electron number density of the plasma. SPECAIR comparisons of the N_2 (2+) system showed average temperatures of approximately 3950 K for T_{vib} and 2050 K for T_{rot} which indicated the non-thermal nature of the plasma as described in [4]. Unfortunately, the Stark broadening analysis yielded no accurate results.

The test bed constructed for the testing of oil burners allowed relative comparisons of the stock and modified burners in an industry-applicable environment. Baseline testing of the stock

burner showed comparable results to that of Riello's standards when taking into account differences in location and a different nozzle size. The stock burner testing results acted as a realistic goal to achieve and exceed with the modified burner. The original results provided by Clean Diesel from over 10 years ago showed significant improvements in fuel efficiency and emissions reduction. In our tests, performance of the modified burner showed no significant improvement in fuel efficiency and therefore no benefit of plasma assisted combustion. While carbon monoxide emissions were reduced by nearly 72% with the modified burner, it also showed increase in nitrogen oxides by 29%. This emissions discrepancy in the two burner types is most likely a result of modifications of the burner rather than effects of the plasma. When the modified burner only used the plasma for ignition (similar to the stock burner), results were nearly identical to that of the burner utilizing plasma for the entire test duration. Since results between plasma ignition and plasma combustion modes were so similar, it was concluded that the change in emission byproducts (relative to the stock burner) was due to the lengthened burner tube or modified turbulator.

A finding from the modified burner testing was that the rate of air and fuel flow through the plasma reduced the volume of plasma to a ring shaped arc. This had two consequences, the first being that most of the mixture passed by the plasma in an unionized region. Secondly, the rate at which the mixture passed by the plasma was fast (estimated to be around 6 m/s), leading to a very small residence time for the mixture to become ionized. The original spherical volume seen at no flow conditions was reduced to a planar ring with the addition of flow, which was not ideal for reformation. Effort was made to make changes to the electrode setup of the burner to allow the plasma to have more interaction with the fuel/air mixture. Initial tests in this regard were not successful, but such approaches are of future interest. Possible areas of future design

improvement include variations to the fuel flow rate (lower flows in particular), turbulator modifications to alter the air-fuel flow mixing, developing schemes for secondary air injection, and developing concepts for pulsed fuel injection.

It is also worth noting that it is possible that there is little room for improvement in the oil burner combustion process. Carbon monoxide emissions were already quite low in the stock and plasma ignition mode tests (less than 40 ppm). If all of this CO was converted into CO_2 with the plasma generator, we would see less than a 0.05% increase in heat release. For the testing results shown in Figure 4-10, an increase of approximately 1% in thermal efficiency would be required to match the plasma generator power input. This means that it may be very difficult for plasma fuel reforming to significantly affect the already efficient combustion process of oil burners, and the thermal efficiency may be improved more effectively by focusing on the heat exchanging properties of the burner/furnace system.

References

[1]   Leonov S. B. and Yarantsev D. A., 2007, "Plasma-induced ignition and plasma-assisted combustion in high-speed flow," Plasma Sources Science and Technology, **16**, pp. 132-138.

[2]   Petitpas G., Rollier J.-D., Darmon A., Gonzalez-Aguilar J., Metkemeijer R., and Fulcheri L., 2007, "A comparative study of non-thermal plasma assisted reforming technologies," International Journal of Hydrogen Energy, **32**, pp. 2848-2867.

[3]   Bittencourt J. A. Fundamentals of Plasma Physics. New York: Springer-Verlag, 2004. Print.

[4]   Staack D., Bakhtier F., Gutsol A., and Fridman A., 2006, "Spectroscopic studies and rotational and vibrational temperature measurements of atmospheric pressure normal glow plasma discharges in air," Plasma Sources Science and Technology, **15**, pp. 818-827.

[5]   Van Veldhuizen E. M., Rutgers W. R., Corona discharges: fundamentals and diagnostics, Retrieved May 17, 2012 from www.phys.tue.nl/FLTPD/invited/veldhuizen.pdf.

[6]   Goldman M., Goldman A., and Sigmond R. S., 1985, "The corona discharge, its properties and specific uses," Pure & Appl. Chem., 57(9), pp. 1353-1362.

[7]   Corona Discharge Image, Retrieved January 28, 2013 from http://www.energeticforum.com/renewable-energy/5637-corona-discharge.html.

[8]   Calvert J. B., 2002, "Electrical Discharges: How the spark, glow, and arc work," Retrieved May 22, 2012 from http://mysite.du.edu/~jcalvert/phys/dischg.htm.

[9]   Glow Discharge Schematic, Retrieved January 28, 2013 from
        http://en.wikipedia.org/wiki/Electric_glow_discharge

[10]   Electric Arc Image, Retrieved January 28, 2013 from
        http://www.scienceclarified.com/Di-El/Electric-Arc.html.

[11]   Roth J. R., 1995, "Industrial Plasma Engineering: Volume I – Principles," Bristol, UK:
        Institute of Physics Press, ISBN 0-7503-0318-2, Section 12.5.2, Section 9.6.3.

[12]   Cambel A. B. and Cambel M. Plasma Physics. Boston: D. C. Heath and Company, 1965.
        Print.

[13]   Brussaard G. J. H., Aldea E., van de Sanden M. C. M., Dinescu G., and Schram D. C.,
        1998, "Evidence for charge exchange between N+ and N2($A^3\Sigma_u +$) in a low-temperature
        nitrogen plasma," Chemical Physics Letters, **290**(4-6), pp. 379-384.

[14]   Laux C. O., Spence T. G., Kruger C. H., and Zare R. N., 2003, "Optical diagnostics of
        atmospheric pressure air plasmas," Plasma Sources and Technology, **12**, pp. 125-138.

[15]   Hopkins M. B., 1986, "Langmuir probe technique for plasma parameter measurement in
        a medium density discharge," Review of Scientific Instruments, **57**, pp. 2210-2217.

[16]   Fantz U., 2006, "Basics of plasma spectroscopy," Plasma Sources Science and
        Technology, **15**, pp. S137-S147.

[17]   NIST database, http://www.nist.gov/pml/data/asd.cfm.

[18]   Staack D., Bakhtier F., Gutsol A., and Fridman A., 2005, "Characterization of a dc
        atmospheric pressure normal glow discharge," Plasma Sources Science and Technology,
        14, pp. 700-711.

[19]   Torres J., Palomares J. M., Sola A., van der Mullen J. J. A. M., and Gamero A., 2007, "A Stark broadening method to determine simultaneously the electron temperature and density in high-pressure microwave plasmas," J. Phys. D: Appl. Phys., **40**, pp. 5929-5936.

[20]   Torres J., Jonkers J., van de Sande M. J., van der Mullen J. J. A. M., Gamero A., and Sola A., 2003, "An easy way to determine simultaneously the electron density and temperature in high-pressure plasmas by using Stark broadening," J. Phys. D: Appl. Phys., **36**, pp. L55-L59.

[21]   Konjevic R. and Konjevic N., 1997, "On the use of non-hydrogenic spectral line profiles for electron density diagnostics of inductively coupled plasmas," Spectrochimica Acta Part B, **52**, pp. 2077-2084.

[22]   Gigosos M. A., and Cardenoso V., 1996, "New plasma diagnosis tables of hydrogen Stark broadening including ion dynamics," J. Phys. B: At. Mol. Opt. Phys., **29**, pp. 4795-4838.

[23]   Gallagher M. J., Geiger R., Polevich A., Rabinovich A., Gutsol A., and Fridman A., 2010, "On-board plasma-assisted conversion of heavy hydrocarbons into synthesis gas," Fuel, **89**, pp. 1187-1192.

[24]   Starikovskiy A. and Aleksandrov N., 2013, "Plasma-assisted ignition and combustion," Progress in Energy and Combustion Science, **39**, pp. 61-110.

[25]   Starikovskii A. Y., 2005, "Plasma supported combustion," Proceedings of the Combustion Institute, **30**, pp. 2405-2417.

[26]   Deminsky M., Jivotov V., Potapkin B., and Rusanov V., 2002, "Plasma-assisted production of hydrogen from hydrocarbons," Pure Appl. Chem., **74**(3), pp. 413-418.

[27]   Hu H., Xu G., Fang A., and Huang W., 2010, "Non-equilibrium plasma assisted combustion of low BTU fuels," Proceedings of ASME Turbo Expo 2010: Power for Land, Sea and Air, Glasgow, UK.

[28]   Turns S. R. An Introduction to Combustion: Concepts and Applications, Third Edition. New York: McGraw-Hill, 2012. Print.

[29]   Paulmier T., and Fulcheri L., 2005, "Use of non-thermal plasma for hydrocarbon reforming," Chemical Engineering Journal, **106**, pp. 59-71.

[30]   Bromberg L., Rabinovich A., Alexeev N., and Cohn D. R., 1999, "Plasma Reforming of Diesel Fuel," Presented at the American Chemical Society Meeting, Anaheim, CA.

[31]   Bromberg L., Cohn D. R., Rabinovich A., and Alexeev N., 2001, "Hydrogen manufacturing using low current, non-thermal plasma boosted fuel converters," Published in the Proceedings of the Symposium on Energy for the 21st Century: Hydrogen Energy, San Diego, CA.

[32]   Bromberg L., Cohn D. R., Rabinovich A., and Heywood J., 2001, "Emissions reductions using hydrogen from plasmatron fuel converters," International Journal of Hydrogen Energy, **26**, pp. 1115-1121.

[33]   Cohn D. R., Rabinovich A., Titus C. H., and Bromberg L., 1997, "Near-term possibilities for extremely low emission vehicles using onboard plasmatron generation of hydrogen," Int. J. Hydrogen Energy, **22**(7), pp. 715-723.

[34]   Lesueur H., Czernichowski A., and Chapelle J., 1994, "Electrically assisted partial oxidation of methane," Int. J. Hydrogen Energy, **19**(2), pp. 139-144.

[35]   Vermeltfoort B. F. W., 2010, "Experimental investigation of plasma assisted combustion using a low-swirl burner," M.Sc. Thesis, Eindhoven University of Technology: Netherlands.

[36]   Jayne M. E., 2005, US Patent No. US2005/0208446 A1, Washington, DC: Smith Patent Office.

[37]   Weinberger H. Residential Oil Burners: 3rd edition, Retrieved February 4, 2013 from http://webtools.delmarlearning.com/sample_chapters/1418073970_ch03.pdf.

[38]   NESCAUM, 2005, "Low Sulfur Heating Oil in the Northeast States: An Overview of Benefits, Costs and Implementation Issues, Retrieved February 4, 2013 from http://www.ct.gov/deep/lib/deep/air/regulations/sip/regionalhaze/final/novattachaa.pdf

[39]   Johnson Burners, "Emissions- Approximate Conversion Factors", Equations Retrieved February 4, 2013 from http://www.johnsonburners.com/resourceeng/Emission%20Conversion%20Factors.pdf

[40]   Riello Burners Model F10 Installation Manual

[41]   Fuel Oil and Combustion Values, Retrieved June 22, 2011 from http://www.engineeringtoolbox.com/fuel-oil-combustion-values-d_509.html.

[42]   Testo 330-1 Flue Gas Analyzer Instruction Manual

Appendix I: SPECAIR Comparison Plots

1 kHz, No Air Flow
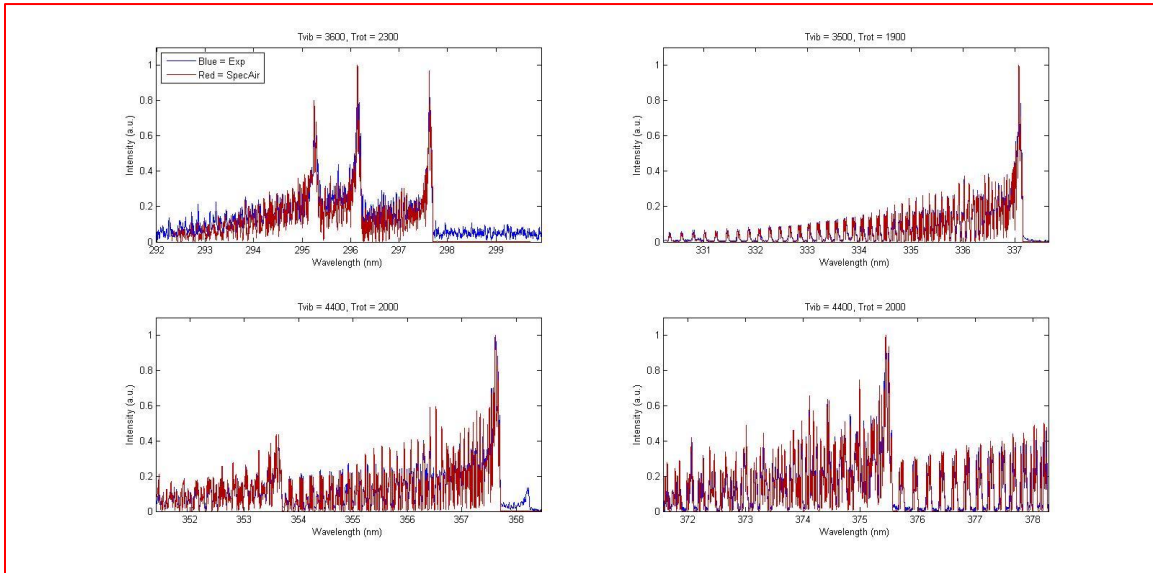
1 kHz, With Air Flow
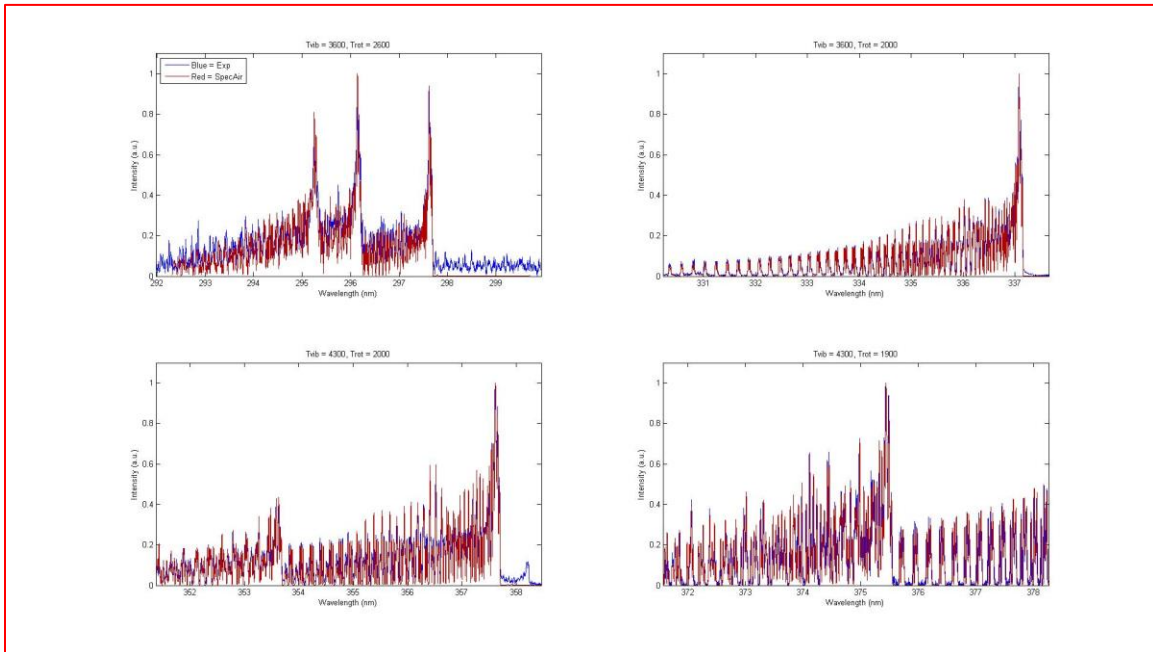
2 kHz, No Air Flow
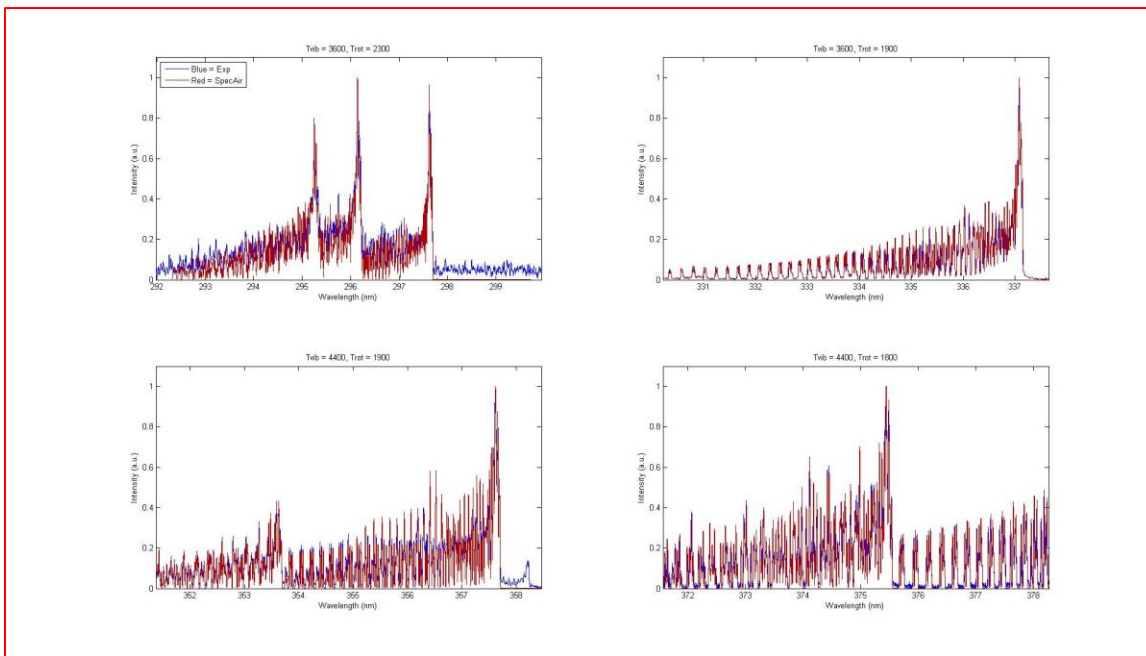
2 kHz, With Air Flow
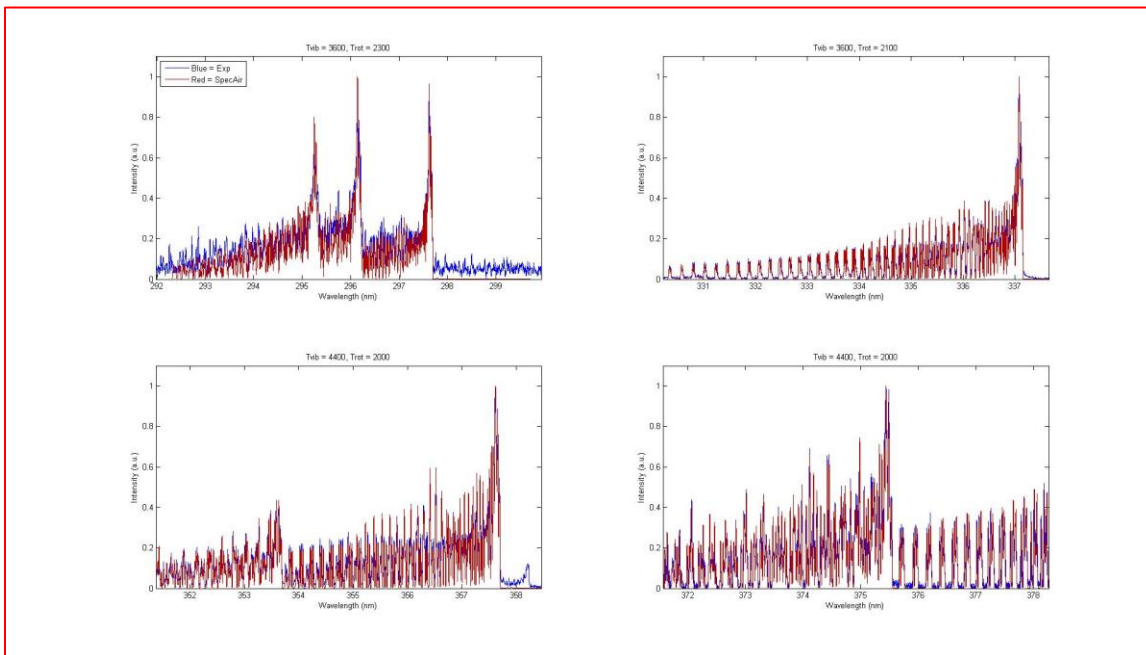
3 kHz, No Air Flow
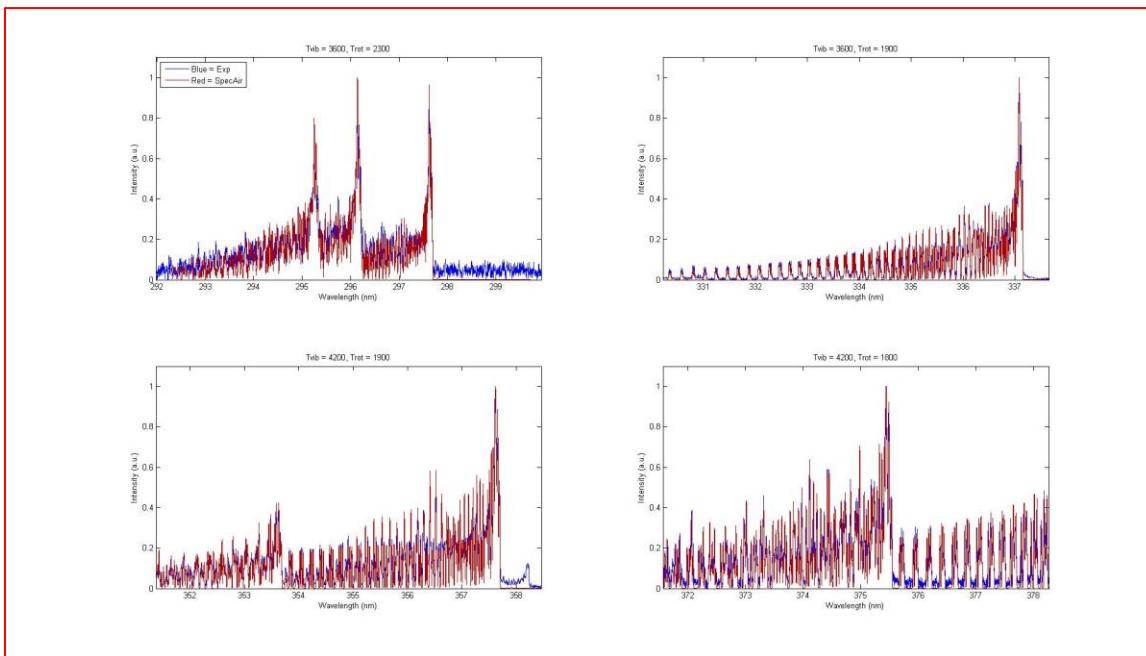
3 kHz, With Air Flow
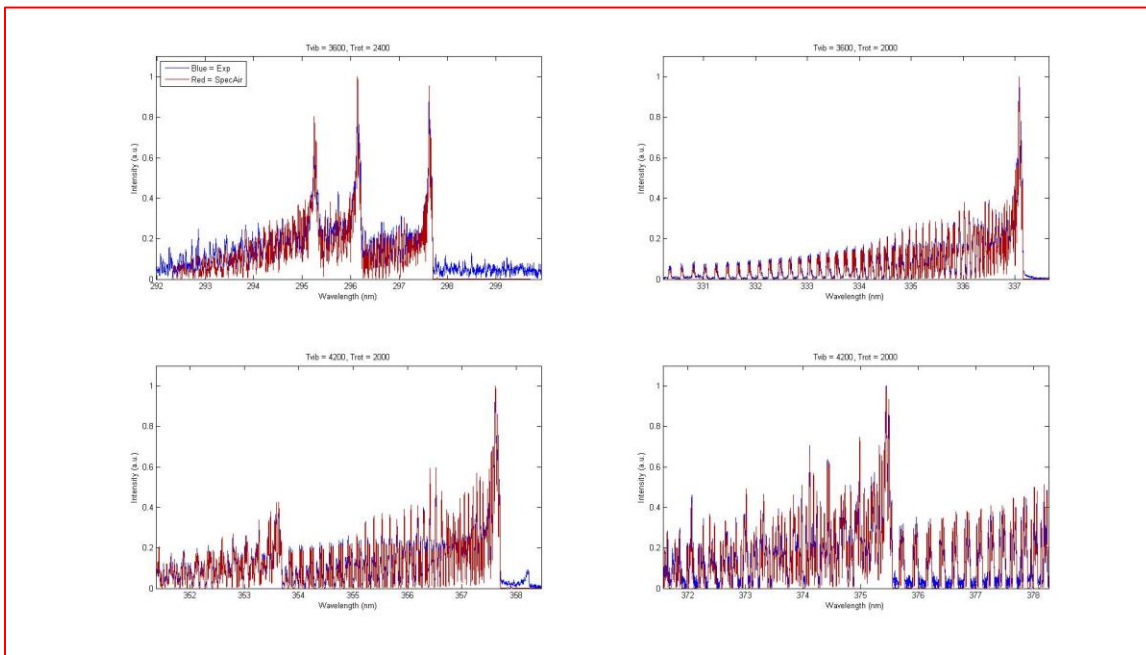
Appendix II: Riello Testing Standards

| RIELLO Riello Burners North America						
	Reference fuel		Oil		Test report n.	0001
	Relative Density @ 60°F	[kg/L]	0,836		Job reference:	Lab Testing
Test specification: Matching	Density (lbs/gal)	[lbs/gal]	6,9747		Standard:	UL726
Burner Type: F10	Viscosity @ 20°C	[mm2/s]	4,50		Date:	Mar 11/2011
S/N: N/A	Stoichometric CO₂	%	15,35		Engineer:	DK
Manufacturer: Pensotti	Degrees API @ 60°F	-	37,80		Approved:	Andrea D.B.
Boiler Type: D-08	Higher Heating Value (HHV)	[Btu/USGal.]	137.120	Motor	Phase	1
S/N: N/A	Higher Heating Value (HHV)	[kWh/kg]	12,703		Volt	120
	Higher Heating Value (HHV)	[Btu/lb]	19660		Frequency	60
Flue size: 6"/rear	Carbon	%	87,02		Ampere	
	Hydrogen	%	12,92		Cos φ	

	#	Measurement or Data Points	Eng. Units	A	B	C	D	E	F	G
Burner Settings	1	Combustion Chamber length	inches							
	2	Flange-Head Position	inches	3.25" to flange						
	3	Single line / Two line	#	2 line	2 line	2 line	2 line	2 line	2 line	
	4	Combustion head setting	#	2	2	2	2	2	2	
	7		Maker	Delavan	Delavan	Delavan	Delavan	Delavan	Delavan	
	8	Nozzle	G.P.H.	1,5	1,5	1,5	1,5	1,5	1,5	
	9		angle/tipe	60°B	60°B	60°B	60°B	60°B	60°B	
Fuel	10	Oil temperature	°F	70	70	70	70	70	70	
	11	Pump pressure	PSI	218	218	218	196	196	196	
	13	Calculated Pump Pressure	PSI	191,53	192,01	194,72	173,82	172,96	174,76	#DIV/0!
	14	Amount of Fuel Measured	GPH	0,16	0,16	0,13	0,16	0,12	0,2	
	15	Time of Fuel Measured	Secs	277,47	277,12	223,59	291,26	218,99	363,09	
	16	Actual Oil Volume Rate	GPH	2,08	2,08	2,09	1,98	1,97	1,98	#DIV/0!
	17	Actual Oil Volume Rate	Lb/h	14,48	14,50	14,60	13,79	13,76	13,83	#DIV/0!
	18	Actual Oil Volume Rate	Kg/h	6,57	6,58	6,62	6,26	6,24	6,27	#DIV/0!
	19	Actual Oil Volume Rate	Btu/Hr.	284.647,4	285.006,9	287.008,2	271.170,5	270.495,6	271.906,1	#DIV/0!
Air	20	Air Setting	°-#	3,9	3,6	5	3,9	3,3	5	
	21	Combustion Head Air Pressure	"w.c.	2,13	1,93	2,5	2,1	1,76	2,53	
	22	Barometric Pressure	"Hg	28,89	28,89	28,89	28,89	28,89	28,89	
	23	Barometric Pressure	mbar	979,1	979,1	979,1	979,1	979,1	979,1	0,0
	24	Room Temperature	°F	73	73	73	73	73	73	
	25	Room Temperature	°C	22,78	22,78	22,78	22,78	22,78	22,78	-17,78
	26	Humidity Relative	%	28	28	28	28	28	28	
	27	Humidity Absolute air	g/kg	4,96	4,96	4,96	4,96	4,96	4,96	#DIV/0!
Flue Gas Emissions	28	Chamber Pressure	"w.c.	0,4	0,34	0,42	0,35	0,3	0,4	
	29	Vent (Breech) Pressure	"w.c.	-0,01	-0,01	-0,02	-0,02	-0,01	-0,04	
	30	CO₂ (Carbon Dioxide)	%	12,95	13,55	12,2	12,4	13,3	11,2	
	31	O₂ (Oxygen)	%	3,28	2,46	4,31	4,04	2,80	5,68	21,00
	32	Air Figure (Lambda)	λ	1,19	1,13	1,26	1,24	1,15	1,37	#DIV/0!
	33	CO (Carbon Monoxide)	ppm	19	40	15	17	25	17	
	34	CO (Corrected to 0% O2)	ppm	22,5	45,3	18,9	21,1	28,9	23,3	0,0
	35	NOx (Oxides of Nitrogen)	ppm	73	74	71	70	70	64	
	36	NOx (Corrected to 3% O₂)	ppm	74,17	71,84	76,60	74,30	69,24	75,26	0,00
	37	NO_x (EN267) correct @ 10g/kg, 20°C	mg/kwh	135,54	137,41	131,80	129,93	129,93	118,73	#DIV/0!
	38	Gross Flue Gas Temperature	°F	357	355	366	348	342	355	
	39	Air Temperature	°F	73	73	73	73	73	73	
	40	Net Flue Gas Temperature	°F	284,0	282,0	293,0	275,0	269,0	282,0	0,0
Media Data	41	Return Media Temperature	°F	94	93	91	89	89	88	
	42	Supply Media Temperature	°F	130	126	124	122	122	119	
	43	Media Temperature Rise	°F	36	33	33	33	33	31	0
	44	Media Pressure	Psig	5	5	5	5	5	5	
Performance Data	45	Total Flue Gas Losses (ANSI)	%	12,85	12,56	13,41	12,88	12,36	13,67	#DIV/0!
	46	Combustion Effy. (ANSI)	%	87,15	87,44	86,59	87,12	87,64	86,33	#DIV/0!
	47	Heat Output (Heating Capacity)	Btu/Hr.	248.071,8	249.222,2	248.506,2	236.244,7	237.064,5	234.733,2	#DIV/0!
	48	Smoke Density (Bacharach)	nr.	0,5	1,0	0-T	0,1	1,0	0-T	
	49	Flame Quality Signal	µA DC							
	50	Ignition Quality	#			Audible/warm			Audible/warm	

NOTE	
TEST A	Rate/13% CO2
TEST B	Min air
TEST C	Max air
TEST D	Field settings
TEST E	Min air
TEST F	Max air
TEST G	

Appendix III: Testo Emissions Calculations

K.5 Principles of calculation

K.5.1 Fuel parameters

Fuel	A2[1]	B[1]	CO_2max	O_2 reference
Natural gas	0,660	0,009	11,8 Vol.%	3 Vol.%
Light oil	0,680	0,007	15,4 Vol.%	3 Vol.%
LPG	0,630	0,008	13,7 Vol.%	3 Vol.%
Wood	0,765	0,000	20,3 Vol.%	13 Vol.%
Pellets	0,765	0,000	20,3 Vol.%	13 Vol.%
Briquette	0,833	0,000	18,9 Vol.%	8 Vol.%
Lignite	0,955	0,000	19,8 Vol.%	8 Vol.%
Anthracite	0,758	0,000	20,5 Vol.%	8 Vol.%
Coke oven gas	0,600	0,011	10,3 Vol.%	3 Vol.%
Town gas	0,630	0,011	13,6 Vol.%	3 Vol.%
Test gas	0,0000	0,000	0,00 Vol.%	0 Vol.%

[1] Fuel-specific factor
[2] Default setting

K.5.2 Calculation formulae

Carbon dioxide:

$$CO2 = \frac{CO_{2max} \times (21\% - O2)}{21\%}$$

CO2max: Maximum carbon dioxide specific to fuel
21%: Oxygen level of air
O2: Measured oxygen level in %

Flue gas loss:

$$qA = \left((FT-AT) \times \left(\frac{A2}{21\% - O2} + B \right) \right) - Kk$$

FT: Flue gas temperature
AT: Ambient temperature
A2/B: Fuel-specific parameters
21%: Oxygen level of air
O2: Measured oxygen level in %
Kk: Calculated value allowing for regained condensate heat if dewpoint level is not reached (for condensing furnaces).

Efficiency:

$$\eta = 100 - qA$$

qA: Calculated flue gas loss

Appendix IV: Best Stock Burner Results with 1.5 GPH Nozzle

Stock Burner Testing Data

	Test Name	12-6b	12-6c	12-6d
	Date/Time	12-6, 11:25 PM	12-6, 11:45 PM	12-6, 12:10 PM
	Sampling Period	11:29:01 - 11:37:21	11:47:00 - 11:56:10	12:12:29 - 12:20:49
Settings	Nozzle Size	1.5	1.5	1.5
	Pump Pressure	146	146	146
	Turbulator Setting	3	3	3
	Air Setting	5.2	5.5	6
Fuel	Avg Fuel Temp	10.34	11.70	9.89
	StDev	0.70	0.54	0.36
	Initial Fuel Mass (kg)	9.79	8.38	13.22
	Final Fuel Mass (kg)	8.73	7.46	12.060
	Time Measured (min)	10.292	9.027	11.486
	Fuel Flow Rate (kg/min)	0.1030	0.1019	0.1010
	Actual GPH	1.9073	1.8873	1.8702
Air	Avg Humidity (%)	29.59	30.57	31.07
	StDev	1.97	3.01	2.90
	Avg Ambient Temp	15.30	16.77	14.91
	StDev	2.21	2.84	1.07
	Air Velocity (ft/min)	1788	1788	1778
	Air Flow Rate (kg/min)	1.864	1.864	1.853
	Air-Fuel Ratio	18.097	18.288	18.352
Heat Transfer	Avg Flow Rate (GPM)	25.83	25.68	25.69
	StDev Flow Rate (GPM)	0.81	0.78	0.75
	Avg dT	7.91	7.93	7.79
	StDev dT	0.36	0.28	0.32
	Q (J/min)	3251715	3241416	3185259
	Q Error (+/-)	179982	150419	161824
	BTU/hour	184922	184336	181143
	BTU/hour Error (+/-)	10235	8554	9203
Emissions	O2 (%)	4.61	4.82	4.93
	StDev	0.04	0.05	0.05
	CO2 (%)	12.26	12.09	12.02
	StDev	0.03	0.04	0.04
	CO (ppm)	16.73	15.56	15.61
	StDev	0.78	0.65	0.73
	NOx (ppm)	88.18	86.13	83.90
	StDev	0.55	0.80	0.65
	Exhaust Temp (TC)	337.12	337.50	337.25
	StDev	0.75	1.14	1.00
	Exhaust Temp Testo	309.51	309.50	309.56
	StDev	2.38	3.01	2.96
	% Excess Air	26.34	27.97	28.70
	StDev	0.30	0.37	0.40
Performance	Combustion Efficiency	81.75	81.64	81.55
	StDev	0.11	0.09	0.10
	Input BTU	267017.892	264227.892	261832.440
	Output BTU	184922	184336	181143
	Output BTU StDev	10235	8554	9203
	Thermal Efficiency	69.25%	69.76%	69.18%
	Thermal Efficiency Error	3.83%	3.24%	3.51%

Appendix V: Burner Testing Procedure

System Preparation:

1. Check the water level of tanks
2. Check that the boiler drain is closed
3. Check that the tank drain is closed
4. Open pump outlet valve
5. Open pump inlet valve
6. Check that the gate valve is open
7. Plug in the pump
8. Plug in the fan
9. Check the level of fuel tank

Data Collection Preparation:

1. Turn computer on
2. Open LV3 VI in the PEIS folder
3. Set Logging Time to at least 60 min
4. Set Logging speed to 1 Hz
5. Run the VI
6. Turn on Testo Analyzer
7. Turn on Pump for the Testo
8. Turn on anemometer in burner duct
9. Turn on fuel scale

Testing Procedure:

1. Start the Data Logger with VI
2. Turn on pump
3. Adjust flow to desired rate
4. Record scale weight
5. Plug in burner/Record starting time/Start timer for fuel flow rate
6. Record Testo data as necessary
7. Record anemometer reading
8. Allow Inlet Temp to reach 70° C
9. When Inlet Temp reaches 70°, turn fan on to High
10. Allow the Inlet and Outlet Temps to stabilize and then continue to run burner for 10-15 minutes
11. Check fuel scale: Record final reading and corresponding timer time
12. Unplug the burner

Shut Down Procedure:

1. After unplugging burner, allow fan to cool water down for a few minutes
2. Stop the Logger on the VI
3. Turn off scale
4. Turn off anemometer
5. Turn off Testo analyzer
6. Turn off pump
7. Turn off fan

Caution:

- **If Outlet Temperature reaches 95°, unplug burner**
- **If water flow rate starts to drop drastically, turn off pump**
- **Keep the window by the burner closed while burner is running**